https://doi.org/10.5194/tc-2020-148
Preprint. Discussion started: 14 July 2020


The Cryosphere Discussions

# Modelling perennial firn aquifers in the Antarctic Peninsula (1979-2016).

J. Melchior van Wessem[1], Christian R. Steger[2], Nander Wever[3], and Michiel R. van den Broeke[1]

[1]Institute for Marine and Atmospheric Research Utrecht, Utrecht University, Utrecht, the Netherlands
[2]Institute for Atmospheric and Climate Science, ETH Zürich, Zürich, Switzerland
[3]Department of Atmospheric and Oceanic Sciences, University of Colorado Boulder, Boulder, CO, USA

*Correspondence to:* J. M. van Wessem (j.m.vanwessem@uu.nl)

**Abstract.** We use two snow models, the IMAU Firn Densification Model (IMAU-FDM) and SNOWPACK, to model firn characteristics in the Antarctic Peninsula (AP). We force these models with mass and energy fluxes from the Regional Atmospheric Climate MOdel (RACMO2.3p2) to construct a 1979-2016 climatology of AP firn density, temperature and liquid water content. A comparison with 75 snow temperature observations at 10 m depth and with density from 11 firn cores, suggests that both snow models perform adequately.

In this study, we focus on the detection of so-called perennial firn aquifers (PFAs), that are formed when surface meltwater percolates into the firnpack in summer, is then buried by snowfall, and does not refreeze during the following winter. In 941 model grid points, covering ∼28,000 $\mathrm{km}^2$, PFAs existed for at least one year in the simulated period, most notably in the western AP. At these locations, surface meltwater production exceeds 150 to 300 $\mathrm{mm\ w.e.\ y}^{-1}$, with accumulation at least an order of magnitude larger.

Most pronounced and widespread are PFAs modelled on and around Wilkins ice shelf. Here, both meltwater production and accumulation rates are sufficiently high to cause PFA formation in most years in the 1979–2016 period, covering a large part of the ice shelf. Other notable PFA locations are Wordie ice shelf, an ice shelf that has almost completely disappeared in recent decades, and the relatively warm northwestern mountain ranges of Palmer Land, where accumulations rates can be extremely large and PFAs are formed frequently.

We find that not only the magnitude of melt and accumulation is important, but also the timing. If large accumulation events occur in the months following an above average summer melt event, this favours PFA formation in that year. Finally, we find that most PFAs are predicted near the grounding lines of the (former) Prince Gustav, Wilkins and Wordie ice shelves. This highlights the need to further investigate how PFAs may impact ice shelf disintegration events, in a similar way as supraglacial lakes do.

## 1 Introduction

The Antarctic Peninsula (AP) is one of the most rapidly changing regions on Earth. In the second half of the 20th century, the lower atmosphere over the AP has warmed up to 3K, which is among the highest warming rates globally (Bromwich et al., 2012), heat content in the surrounding ocean has significantly increased (Schmidtko et al., 2014), as well as precipitation rates

https://doi.org/10.5194/tc-2020-148
Preprint. Discussion started: 14 July 2020


(Thomas et al., 2008), and most perennial sea ice has disappeared (Stammerjohn et al., 2011). Largely as a result of these changes, 90% of its glaciers are retreating and ice shelves on both sides of the AP have disintegrated or have shown area loss and thinning (Cook et al., 2014, 2016). Rising atmospheric temperatures increase surface meltwater production which has been linked to ice shelf disintegration, as it depletes firn air content and can hydrofracture the ice shelf when the meltwater fills pre-existing crevasses (Scambos et al., 2000; Van den Broeke, 2005). It is therefore pivotal to correctly model the pathway of meltwater when it enters the firn. For long it has been assumed that meltwater in Antarctica either refreezes immediately in the firn, runs off directly into the ocean, or forms supraglacial lakes (melt ponds) on the ice shelf surface. However, liquid meltwater can also be retained in the firn even during winter without refreezing. These so-called perennial firn aquifers (PFA) are extensive on the Greenland ice sheet (Forster et al., 2013) and can reduce and delay runoff (Kuipers Munneke et al., 2014a). In the AP, PFAs could potentially impact processes related to ice shelf hydrofracturing when meltwater is stored in the firn before it percolates into crevasses (Bell et al., 2018; Alley et al., 2018). Firn aquifers could also enhance surface meltwater transport to the ice sheet base having a lubricating effect on glaciers (Bell et al., 2018), or affect ice rheology of both grounded ice and ice shelves through latent heat release (Hubbard et al., 2016).

No (published) observations or model simulation of firn aquifers currently exist for Antarctica. In Greenland, PFAs are found in regions which combine high accumulation with high surface melting (Kuipers Munneke et al., 2014a). When accumulation, which is the sum of snow sublimation and snowfall, is sufficiently large it can bury and isolate the summer meltwater from the winter cold wave, preventing refreezing. Kuipers Munneke et al. (2014a) suggested optimal PFA conditions are accumulation rates between 1000 and 3000 $\mathrm{mm\ w.e.\ y^{-1}}$, and sustained melting in summer. These conditions prevail in the (western) AP, where snowfall rates are generally high due to orographic precipitation. Additionally, the AP is the northernmost and therefore warmest region in Antarctica, with significant surface melting in summer (Van Wessem et al., 2016) and even in winter (Kuipers Munneke et al., 2018). Its climate is therefore relatively similar to that of southeast Greenland, where extensive PFAs have been observed as well as modelled (Forster et al., 2013; Steger et al., 2017a; Brangers et al., 2020).

In this study, the firn and possible PFA conditions in the AP are assessed using two snow models; IMAU-FDM (Ligtenberg et al., 2011) and SNOWPACK (Bartelt and Lehning, 2002). The models are forced by realistic atmospheric and surface conditions from the regional climate model RACMO2.3p2 for the period 1979–2016, which has been extensively evaluated with several observational datasets (Van Wessem et al., 2018). This combination of models accurately simulates PFA locations in Greenland (Forster et al., 2013; Steger et al., 2017a). Section 2 introduces the model and observational datasets used for evaluation. Section 3 evaluates the model output using available observations of firn density and temperature, while section 4 focuses on the differences between SNOWPACK and IMAU-FDM. Section 5 treats the specific PFA characteristics of the AP. Section 6 provides a discussion of results and future prospects of meltwater modelling in the AP, followed by conclusions in Section 7.

https://doi.org/10.5194/tc-2020-148
Preprint. Discussion started: 14 July 2020


## 2 Data and Methods

Two snow models are used, the Institute for Marine and Atmospheric research Utrecht firn densification model (IMAU-FDM) (Ligtenberg et al., 2011) and SNOWPACK (Bartelt and Lehning, 2002; Lehning et al., 2002). The RACMO2.3p2 regional atmospheric climate model is used to force these models offline. As a third comparison product, the snow model from RACMO2.3p2 is used directly, which is a low resolution version of the IMAU-FDM. All three models and their forcing are described below.

### 2.1 Regional Atmospheric Climate Model RACMO2.3

The Regional Atmospheric Climate Model RACMO2.3p2 combines the dynamical processes of the High Resolution Limited Area Model (HIRLAM) (Undén et al., 2002) with the physics package of the European Centre for Medium-range Weather Forecasts (ECMWF) Integrated Forecast System (IFS). RACMO2.3p2 includes a multilayer snow model that calculates melt, percolation, refreezing and runoff of liquid water (Ettema et al., 2010); it is a 100-layer version of the IMAU firn densification model (FDM) that is described below. RACMO2.3 also uses a prognostic scheme for snow grain size used to calculate surface albedo (Kuipers Munneke et al., 2011); and a drifting snow routine that simulates the interaction of drifting snow with the surface and the lower atmosphere (Lenaerts et al., 2012). The model has been applied at a relatively high horizontal resolution of $\sim$5.5 km over the AP, and has 40 vertical atmospheric levels. At the lateral atmospheric boundaries the model is forced by ERA-Interim reanalysis data, and at the ocean surface by prescribed ocean surface temperatures and sea ice cover. The model atmosphere is initialised on Jan. 1st, 1979 using the ERA-Interim reanalysis data. Further details about RACMO2.3p2 and the evaluations in the AP are provided in Van Wessem et al. (2015, 2016, 2018).

### 2.2 IMAU-FDM

This semi-empirical model was described in detail in Ligtenberg et al. (2011), and this section only repeats the main characteristics. The model consists of layers of varying thickness, of which the properties (temperature, mass, density and liquid water content) are followed in a Lagrangian way through the firn pack. The vertical water motion is simulated using the bucket scheme, in which meltwater moves through all layers within a single model time step; water is retained as ice or liquid water based on the firn porosity and cold content. The irreducible water content is set to a relatively low value of 2% of the pore volume allowing meltwater to efficiently percolate down to lower layers, mimicking processes such as piping and meltwater retention. The model only allows meltwater to be retained through the irreducible water content and does not allow water ponding on superimposed ice; if liquid water reaches the firn-ice boundary, it is assumed to run off directly. The FDM is forced using three-hourly fields from 1979 to 2016 of accumulation (the sum of snowfall and sublimation), snow erosion, 10 meter wind speed, surface temperature and snowmelt from RACMO2.3p2 (Van Wessem et al., 2018). The lower firn boundary condition for the heat equation was set as a Neumann zero-flux boundary condition, which is a good assumption in the deep firn where gradients are expected to be negligibly small (Ligtenberg et al., 2011).The initial firn pack is generated by forcing the FDM as many climatological periods (1979-2016) as needed to refresh the entire firn layer. The spin up time depends on the depth of the firn layer, which in turn depends on the average accumulation and snowmelt at the respective grid point, and therefore

https://doi.org/10.5194/tc-2020-148
Preprint. Discussion started: 14 July 2020


varies spatially. The final initialisation product is in near-balance with the average climate, and provides the best estimate of the initial state of the AP firn pack.

### 2.3 SNOWPACK

SNOWPACK is a microphysical snow model originally designed to model seasonal snow cover in alpine areas (Bartelt and Lehning, 2002; Lehning et al., 2002). It has recently been applied successfully to the Greenland Ice sheet (Steger et al., 2017b). In that study, a simplified version of SNOWPACK using a bucket scheme for meltwater percolation was used to reduce computational costs and to allow comparison with the IMAU-FDM. Water ponding is not allowed in the version used here, and meltwater retention is simulated using an irreducible water content depending on temperature, and averages 4% by volume. For further details we refer to Steger et al. (2017a, b). In this study, besides using a new version of SNOWPACK, the main change from the Greenland simulation is the forcing mode. In this study the model calculates its own surface energy budget (SEB), instead of using direct forcing with surface temperature and mass fluxes, as this yielded better results for the AP. Three-hourly fields from RACMO2.3p2 for 1979–2016 of precipitation, downwelling and upwelling shortwave- and longwave radiation fluxes, 10 m wind speed, 2 m air temperature and specific humidity are used (Van Wessem et al., 2018). As both the up- and downward shortwave fluxes are prescribed, this automatically sets the surface snow albedo. The turbulent (sensible and latent heat) fluxes are based on the bulk method and are calculated using near-surface temperature and humidity gradients. These fluxes are then used to calculate sublimation/deposition and evaporation/condensation. As in IMAU-FDM, the lower firn boundary condition for the heat equation was set as a Neumann zero-flux boundary condition. The model is spun up in a fashion similar to the IMAU-FDM. In general, densification in SNOWPACK is slightly weaker than in IMAU-FDM (Steger et al., 2017a) and as a result SNOWPACK spinup for some locations does not refresh the full firn layer. The effects on the results on this study are undetectable. There are some datagaps in the SNOWPACK simulations due to model crashes as a result of very thin snow layers in dry high and cold high elevation regions, but these did not effect the conclusions of this study.

### 2.4 Observational data

#### 2.4.1 10 m firn temperature

This study uses 10 m firn temperatures from the Surface Mass Balance and Snow Depth on Sea Ice Working Group (SUMup) (Montgomery et al., 2018) for model evaluation (Fig. 1). All observations applicable to this study have unfortunately been obtained prior to the starting year of the simulations (1979) and cannot directly be matched with the model results; hence the climatological average from 1979–2016 is used for modelled firn temperature. Using earlier averaging periods does not yield significantly different results. Measurements that are not located on a RACMO2 landice grid point or that are located on ice shelves that have disintegrated before 2008 are not included, resulting in 75 observations used. All observations are corrected for any discrepancies in model elevation using a temperature lapse rate of 7.2 $\mathrm{K\ km^{-1}}$ (Morris and Vaughan, 2003).

https://doi.org/10.5194/tc-2020-148
Preprint. Discussion started: 14 July 2020


#### 2.4.2 Density profiles from Larsen C

The model performance in simulating density profiles is evaluated using observations from 11 firn cores from the Larsen C ice shelf (Table 1). Six shallow to medium-deep density observations as reported in Munneke et al. (2017) are used. J1, J2 and J3 reach up to 30 m depth and were collected in 2009 using a neutron-scattering probe with a vertical resolution of 10 cm. LAR1, LAR2 and LAR3 are 6 m deep firn drillings, also from the 2009 field season. The other five observations are deep (100 m depth) firn profiles collected with optical televiewing (OPTV) of hot-water drilled boreholes as described in Ashmore et al. (2017), with 1 cm vertical resolution.

## 3 Results: Evaluation

### 3.1 10 meter firn temperature

Figure 2 compares observed with modelled SNOWPACK (blue) and IMAU-FDM (red) 10 m firn temperature $T_{10m}$. SNOWPACK and IMAU-FDM simulate snow temperatures with comparable skill: $r^2$= 0.91; 0.85, RMSD = 1.55;1.89 K and slope = 0.90; 0.80, respectively. As an extra comparison, RACMO-FDM snow temperatures are shown, which, as expected, are similar to those generated by the IMAU-FDM. SNOWPACK performs best at simulating the higher temperatures, found in locations with summer melt and significant firn warming due to refreezing. At colder locations, firn temperature is somewhat overestimated. Both models on average underestimate 10 m snow temperature, which is partly related to known errors in the atmospheric forcing; i.e. underestimated downwelling longwave and shortwave radiation. These biases largely explain the underestimation in surface melt production in both models (Ligtenberg et al., 2018; Van Wessem et al., 2018). There are only limited observations with $T_{10m} > 265$ K; here melt rates are high ($> 500$ mm w.e. $y^{-1}$) and as a result the firn layer is either shallow, or absent. At these locations, the modelled $T_{10m}$ represents ice temperature. There are also a few outliers for both models; these represent locations on steep slopes, likely with complex atmospheric and surface conditions not resolved by the model.

### 3.2 Density profiles

Figure 3 compares modelled and observed density profiles on Larsen C ice shelf and lists FAC; vertically integrated pore space over the firn column. The shallow cores in the upper panel show good agreement. SNOWPACK typically models a larger FAC than IMAU-FDM, which results in a better match with the observations, e.g. cores J1_08, LAR1 and LAR3. As the (output) vertical resolution of SNOWPACK in our setting is coarse, due to the aggressive layer merging necessary for optimisation of computation time, IMAU-FDM shows larger variability. For the deeper cores, which reach considerably higher densities than the shallow cores, the IMAU-FDM performs better, especially for the CI-cores, simulating several layers of ice that agree with the observations. FAC simulated by SNOWPACK is too high, which is most critical for the two WI cores. Here, both models deviate strongly from the observations, especially in the upper 40 m, where the observations represent a vertical profile that almost completely consists of ice. This is likely related to these locations being located in shallow surface depressions,

https://doi.org/10.5194/tc-2020-148
Preprint. Discussion started: 14 July 2020


with lateral advection of meltwater from adjacent locations, a process that is not represented by the 1D-models. For ice cores with high melt rates (J1_08, LAR1, LAR2, CI120, CI22) the performance of SNOWPACK is compared to locations with low melt rates, consistent with the results in the previous section. This confirms that rysnow densification is underestimated by SNOWPACK.

## 4 Results: IMAU-FDM and SNOWPACK

As the accumulation forcing is largely identical except for minor differences in sublimation, most differences between the models derive from the firn densification and percolation schemes. Where IMAU-FDM uses meltwater production rates prescribed by RACMO2, SNOWPACK calculates its own surface energy budget and therefore melt rates. Figure 4 shows the major firn climatologies with a focus on the intermodel differences.

Figures 4a-c show the modelled FAC of the IMAU-FDM (a) and SNOWPACK (b) and the difference (c). The calculated FAC is shown for the first 30 meters only, disregarding the deeper layers, enabling a more useful comparison as meltwater percolation mostly affects the upper firn. The overall pattern is similar in both models. In warmer regions with sustained surface melting (see Figs. 4g,h), mostly over the Larsen C, George VI and Wilkins ice shelves, FAC is low, with values approaching 1 m, SNOWPACK simulates larger FAC than the IMAU-FDM, whereas in regions with large FAC (i.e. large accumulation rates and/or little melt), such as the western mountain range of Palmer Land and several high elevation locations to the south, SNOWPACK generates lower values. This reflects the stronger dry snow densification in IMAU-FDM.

Figures 4d-f compare simulated 10 m firn temperature , illustrating the generally warmer firn conditions simulated by SNOWPACK. This is a uniform pattern over the AP, with only some locations where IMAU-FDM $T_{10m}$ is higher. Figs. 4g-i show that melt rates are largely similar. IMAU-FDM generally somewhat simulates larger values ($\sim$25 $\mathrm{mm\ w.e.\ y^{-1}}$) than SNOWPACK, except over George VI and Wilkins ice shelves, and near the former Prince Gustav ice shelf. These differences in melt are explained by differences in the turbulent heat fluxes (not shown), but overall the differences are small (less than 10%). Finally, Figs. 4j-l show the average vertically integrated liquid water content (LWC), which represents the meltwater that is not refrozen or does not runoff in the same model timestep. The patterns of LWC are similar to those of meltwater production in both models: LWC is mainly concentrated on the ice shelves and towards the north. Values are generally lower than the surface meltwater availability, as most meltwater refreezes, even in summer. This is clearest on Larsen C ice shelf, where only a small fraction of meltwater remains liquid. Note that these figures do not represent PFAs; for these, liquid water must still be present after winter. These locations are discussed in Section 5.

The LWC differences between the two models do not always coincide with those in surface melt rates. For instance, over some parts of Wilkins ice shelf, where absolute values of LWC peak, SNOWPACK LWC can be smaller than in IMAU-FDM, while the melt is actually higher, as is the case for other regions with high surface melt such as near the former Prince Gustav ice shelve. Likely the firn layer is completely (or to a greater depth) filled with meltwater, and as in SNOWPACK the firn porosity and firn depth is larger, LWC is larger. Due to the higher irreducible water content in SNOWPACK, it is retained in upper layers of the firn longer.

https://doi.org/10.5194/tc-2020-148
Preprint. Discussion started: 14 July 2020


In summary, both models behave similarly, but small differences as described above remain. Importantly, several locations exist where both models predict that the meltwater does not refreeze or runoff to the ocean, but is in fact retained as liquid water in the firn layer even outside the summer season, suggesting the presence of perennial firn aquifers. This will be the focus of the next section.

## 5 Results: Perennial firn aquifers (PFAs)

Figure 5 shows the annual average vertically integrated LWC for those grid points with PFA presence, i.e. where liquid water is persistent throughout at least one hydrological year (October to September of the next year in the period 1979-2016). In total, 796 IMAU-FDM and 864 SNOWPACK model grid cells conform to this definition, with 941 grid cells having a PFA in either of the two models, which corresponds to an area of roughly 28,000 $\mathrm{km}^2$ where a PFA has existed at least a year in either of the models, approximately 50% when compared to the ∼55,000 $\mathrm{km}^2$ in Greenland (Brangers et al., 2020). PFA grid cells with LWC reaching high values ($> 1000\mathrm{kg\ m}^{-2}$) occur mainly on the western slopes in northwest Palmer Land where accumulation as well as melt rates are relatively large. The two models largely agree in most areas, but IMAU-FDM shows larger LWC. The Wilkins ice shelf stands out as the main PFA region, with a peak in LWC in the north of the ice shelf, and an additional peak in Schubert inlet. Towards the ice shelf interior, where surface melting is weaker, LWC decreases.

PFA grid points are also predicted by both models along the entire western AP from Wilkins ice shelf towards the northern tip of the AP. In many of these locations, both models generate peak LWC values $>1000\ \mathrm{kg\ m}^{-2}$. In the eastern AP the models simulate PFAs in a few isolated locations on the grounded ice near the remnants of Larsen A and Prince Gustav ice shelves, with low LWC values. The Larsen B embayment shows a significant difference between the models; IMAU-FDM does not predict any PFAs here, whereas SNOWPACK does. Here, LWC values are low ($<30\ \mathrm{mm\ w.e.\ y}^{-1}$), PFAs usually only last one year and water is not found deeper than 10 m (not shown). The difference between the two models is mainly explained by the difference in irreducible water content; in IMAU-FDM the meltwater is vertically distributed along the firn quicker, after which it refreezes more easily.

Figure 6 shows the persistence of the PFAs as a fraction of total years (1979–2016) in which the PFA occurs. For Larsen B, the small PFAs are only present during $<5$ % ($<2$ years) of the in total 38 years. For the other PFAs the pattern reflects that of LWC: in some locations the PFA is present during the entire period, but for most locations the PFAs occur intermittently: during cold periods with less melt PFAs are not formed, liquid water refreezes in the firn, or the meltwater in the firn runs off as it encounters an ice layer.

Figure 7 shows the yearly surface area of PFAs during 1979–2016, and the yearly average melt (of both models) and accumulation for these grid points. Note that MAU-FDM and SNOWPACK snowmelt rates are roughly similar, averaged at PFA locations, albeit SNOWPACK values are slightly higher (∼5%) in some years. Because of these minor differences, throughout the rest of this study the melt forcing of RACMO2/FDM is used for simpler visualisation.

The largest area of PFAs is found in the 90s, with a peak of ∼19,000 $\mathrm{km}^2$ in 1998. During the last decade, snowmelt has decreased, which is related to atmospheric cooling over the AP (Van Wessem et al., 2015; Turner et al., 2016), and PFA area

https://doi.org/10.5194/tc-2020-148
Preprint. Discussion started: 14 July 2020


diminishes as liquid water gradually freezes.. LWC values in IMAU-FDM are $\sim$ 20% larger than in SNOWPACK, as is the area of PFAs. This difference is largely explained by the difference in PFA extent on Wilkins ice shelf. The temporal variability in both models is similar.

It does not appear there is a clear relation with either annual averages of accumulation or snowmelt, but some relation is suggested. For instance, there is a clear relation between periods of PFA area growth when average melt exceeds $\sim$400 $\mathrm{mm\ w.e.\ y^{-1}}$, or about 25% of the annual average accumulation, such as in 1986-1989 or 2005-2006. Therefore, a more detailed analysis will be provided below. It is also interesting that SNOWPACK simulates PFAs over a larger number of grid points ( 864 vs 796) while having a smaller surface area than IMAU-FDM annually; apparently in some years SNOWPACK models some small PFAs while IMAU-FDM does not, such as in the Larsen A and Larsen B embayments.

The subtle interplay between surface meltwater production and accumulation in PFA formation is illustrated in Figures 8 and 9. This analysis follows Kuipers Munneke et al. (2014b) who found in an idealised experiment that PFAs form in relatively warm locations with sufficient surface meltwater production, but are also highly sensitive to accumulation rates. Figure 8 shows the climatological distribution of RACMO2 grid points for binned yearly melt and accumulation. The vast majority of grid points falls in the lower left corner, with modest melt and accumulation rates. Numbers quickly drop for larger melt and accumulation rates. Figures 8b,c show the same distribution as in a), but now only for PFA grid points and years; i.e. with liquid water in the firn during a full hydrological year. Numbers are much lower; a peak of $>$100 points is found in both models at a melt rate of 400 $\mathrm{mm\ w.e.\ y^{-1}}$ and an accumulation rate of 750 $\mathrm{mm\ w.e.\ y^{-1}}$. Figure 8d,e visualizes the PFA occurence fraction; i.e. the PFA count (b,c) divided by the total amount of model grid points (a). PFAs are clearly favoured by high melt and high accumulation conditions located in the top right corner, but these conditions are at the same time relatively rare.

Figure 9 focuses on PFA formation, by showing the same distribution as in Figs. 8b,c, but now only years in which a PFA is formed or has increased in size are taken into account. This means that years in which a PFA shrinks are not considered, even though the PFA may still be present. Figures 9a,b show that PFA formation is restricted to higher melt and accumulation rates compared to PFA presence (Fig. 8); PFAs are only (significantly) formed/grown at melt rates $>$150 $\mathrm{mm\ w.e.\ y^{-1}}$ and for accumulation rates of $>$500 $\mathrm{mm\ w.e.\ y^{-1}}$. Extending the criteria as before to PFA fraction of total grid points (Fig. 9c,d) no distinct optimum is seen, apart from a local maximum for accumulation rates ($<$1500 $\mathrm{mm\ w.e.\ y^{-1}}$) and a melt rate of 550 $\mathrm{mm\ w.e.\ y^{-1}}$. Towards the top right, conditions are found where close to 100% of the time PFAs are formed, but the number of points is small. Both models simulate roughly the same PFA behaviour, but for SNOWPACK maxima are found for a larger number of conditions.

Finally, Figures 9d,e show the fraction of summer meltwater that is retained in the firn layer at the end of winter, only when positive and above 5%. This better shows the efficiency of the firn to prevent refreezing of subsurface meltwater. Even though the pattern shown is similar to Figs 9c,d, there is a clearer dependency on the isolating effects of accumulation. This shows that at higher accumulation, the fraction of meltwater that is retained increases, and the more efficient PFAs are formed and/or grown in subsequent years. This also illustrates the sensitivity of locations for future changes in melt and accumulation rates.

https://doi.org/10.5194/tc-2020-148
Preprint. Discussion started: 14 July 2020


Were these rates to increase, especially those of accumulation, it is likely that more PFAs will be formed and more meltwater buffered in the firn (and potentially transferred to rifts and crevasses).

### 5.1 Results: Case studies at three aquifer locations

Three specific PFA locations are selected for case studies. The locations and their climatic conditions are shown in Figs. 5 and 8, respectively.

#### 5.1.1 Wilkins ice shelf

In both models, Wilkins ice shelf (WIS) has the most prominent PFA signature of the AP. The presence of liquid water in the firn is confirmed by in-situ observations (Scambos et al., 2009). Figures 8,9 identify WIS as a site with favourable conditions in terms of accumulation and surface melt water production. This is also a region where significant supraglacial water (melt ponds; Scambos et al., 2009) and saturated firn (Alley et al., 2018) have been observed. Figure 10 shows a time serie of volumetric LWC profiles from both SNOWPACK and IMAU-FDM for one location with annual LWC $>500\ \mathrm{kg\ m^{-2}}$(Fig. 5). This particular location is not necessarily representative of the entire PFA system of the shelf, which is variable in water content and retention depth, but constitutes a PFA with large interannual variability and is therefore most interesting for a case study. PFAs are formed in both models in several years. The most significant ones, where more than 5% of the meltwater is retained, are highlighted with grey bars in Fig. 10. 1984/1985 is the first year in which meltwater penetrates to $\sim$10 m depth in both models, and is retained throughout the entire following year, but then refreezes the next year. PFA formation at WIS is most significant in the relatively warm 1990s, during which the PFA is growing and extending deeper in the firn pack, lasting until 2005 in SNOWPACK, and 2009 in IMAU-FDM. After that, as temperatures decrease, the liquid water refreezes at this site.

Figure 10c shows local monthly accumulation and melt, highlighting the years of PFA formation. In those years melt rates are above average, as shown by the horizontal lines that represent the mean plus one standard deviation thresholds, and enough meltwater is available to initiate or grow a PFA. It also appears that accumulation rates in the months after these melt peaks are often higher than average, but not as evidently so.

#### 5.1.2 Wordie ice shelf

Only 10% of Wordie ice shelf remains in 2008 when compared to the 1960s, with the largest area decrease in the 1990s (Cook et al., 2014). This makes it an interesting case to explore potential impact of PFA formation on ice shelf stability. Figure 5 shows PFAs presence near the grounding line, with considerably larger LWC in IMAU-FDM than in SNOWPACK. Figure 11 shows the volumetric LWC for one of these locations. IMAU-FDM simulates a PFA over the whole period, growing significantly from 2002 onwards and extending even below 50 m depth, while SNOWPACK only shows a marginal aquifer in the late 90s and early 00s. As the local melt-fluxes in both models (Figs. 4g) are similar, this difference is most likely related to the formulation of the irreducible water content in both models. Because SNOWPACK has a larger percentage (4% vs 2%), the meltwater

https://doi.org/10.5194/tc-2020-148
Preprint. Discussion started: 14 July 2020


is retained longer in the upper layers where it can be more efficiently refrozen by the winter cold wave. This effect may be amplified by the spin up of the models; a colder firnpack has more potential for refreezing.

In Fig. 11c, the monthly melt and accumulation rates do not show a clear formation mechanism, but the combination of high melt with high accumulation afterwards is visible in some years.

#### 5.1.3 Palmer Land

The most robust presence of PFAs in both models is in the northwest mountain range of Palmer Land; where accumulation rates reach up to several meters water equivalent per year. This area also experiences considerable surface melting being located far north and without much sea ice cover year-round. Figure 5 identifies many PFAs, many reaching LWC values above $>$1000 $\mathrm{kg\,m^{-2}}$, mostly over the islands and the (north)west facing slopes. One of these locations is shown in Figure 12, with an accumulation rate of 5.1 $\mathrm{m\ w.e.\ y^{-1}}$ and a relatively low melt rate of 240 $\mathrm{mm\ w.e.\ y^{-1}}$(see Fig. 8). Nearly every year up to 2008 a PFA develops, but not many are retained longer than about 1.5 years. This is caused by the extreme accumulation rates that deeply bury the summer meltwater, as evident from the steep slopes of LWC fraction with respect to time. Because most snow falls at subzero temperatures, these deep snow layers have sufficient cold content to refreeze the meltwater from above and below. The strong firn compaction caused by the high accumulation rates also causes a reduction of the amount of liquid water that can be retained in a snow layer, which results in some extra water loss through melt water runoff, which is otherwise rare in Antarctica. This behaviour is seen for most PFA locations in this region that have melt rates below approximately 300 $\mathrm{mm\ w.e.\ y^{-1}}$. On the islands melt rates are (much) higher, and here PFAs are found that almost completely fill the firnpack, hence the large LWC values in both models. For Palmer Land, LWC in both firn model simulations is comparable.

Fig. 12c shows the extremely large accumulation rates, which are an order of magnitude larger than melt. As accumulation is so large, it is most of the time sufficient to isolate the summer meltwater. Only in years where both accumulation and melt are relatively low, no PFAs are formed.

## 6 Discussion

### 6.1 Intermodel differences

This model study shows the significant potential for the presence of perennial firn aquifers (PFAs) in the AP. They are predicted to occur mostly in the western AP where both melt and accumulation rates are large. The results are largely coherent between the IMAU-FDM and SNOWPACK firn models, but in some regions, most notably near the former Wordie ice shelf, large differences were found, and on average the IMAU-FDM simulates deeper PFAs and higher LWC values. Intermodel differences can be mainly ascribed to differences in the irreducible water content, but also by differences in surface melting, snow densification parameterizations and the firn pack initialization; the accumulation forcing for both models is equal.

IMAU-FDM has a fixed irreducible water content of 2%, substantially lower than (the snow temperature dependent) irreducible water content in SNOWPACK, which averages 4%. As a result, more water can be retained near the surface after

https://doi.org/10.5194/tc-2020-148
Preprint. Discussion started: 14 July 2020


melting, which increases the refreezing potential before it percolates to greater depths (Steger et al., 2017a) . Additionally, the spinup of both models is different. The spin-up time of IMAU-FDM is dependent on the yearly average snowfall and surface melt production, so as to rebuild the entire firn layer. For SNOWPACK the same approach is used, but, with firn densification being weaker in SNOWPACK, the spin up does not replace the entire firn profiles. Longer spinups were not performed due to computational costs. This also results in some of the SNOWPACK initial firn profiles to be colder than in IMAU-FDM, having more potential for refreezing the meltwater penetrating in the firn. However, this effect is likely only present for few locations in this study, and mostly applicable to dry and cold regions where PFAs do not form.

### 6.2 Firn air content, lateral meltwater and superimposed ice

Section 3 showed large discrepancies between models and observations for some locations on Larsen C ice shelf: modelled densities are too low (and firn air content too high) for cores WI-0 and WI-70, which may apply to other regions as well. Combined with both models being, on average, too cold, this potentially reflects lateral flow of meltwater, which is not considered in the snow models. Hubbard et al. (2016) found deep/thick ice layers in the firn and related these to gentle depressions in surface topography causing meltwater to accumulate from surrounding locations, which also explains the extensive melt ponds (Kingslake et al., 2017). Future research should focus on incorporating these effects in firn models, for instance using Alpine 3D (Lehning et al., 2006) which allows lateral movement of meltwater, or incorporating processes that affect meltwater percolation, such as (horizontal) piping (Reijmer et al., 2012), preferential flow (Wever et al., 2016) or subsurface radiation penetration and melting (van Dalum et al., 2018). Many of the PFAs in this study are found near the grounding line, often on grounded ice, so that horizontal meltwater transport can also transport the PFA meltwater towards the ice shelves with additional implications for their stability (Lenaerts et al., 2016).

On the other hand, Holland et al. (2011) and Kuipers Munneke et al. (2014b) suggested that modelled firn air content on large parts of Larsen C ice shelf is too low, caused by either meltrates that are overestimated, or accumulation rates that are too low, or both. This can also be related to how deep the meltwater penetrates into the firn and how important the sensitive melt-albedo feedbacks (Jakobs et al., 2018) is. Obviously, to tackle these problems, more observational constraints are needed.

Finally, both firn models currently lack a realistic physical representation of meltwater retention: they only retain meltwater in the firn due to irreducible water. In reality, meltwater is also retained due to the ponding on top of superimposed ice (slush), similar to the formation of melt ponds. This process presently is not included in the model versions used and thus the current approach should be regarded to be a first order estimate of firn processes and aquifer locations (Ligtenberg et al., 2011; Steger et al., 2017a).

### 6.3 PFA seasonality

Sections 5.1.1-5.1.3 showed the evolution of PFAs for three locations. It is clear that for PFA formation accumulation and melt rates should be high enough, but the monthly time series shown in Figures 10-12c suggest that the timing of accumulation could also play a major role. Figure 13 shows the seasonality of monthly melt and accumulation for the extreme PFA formation years (solid lines) where more than 25% of meltwater is retained at the end of winter, i.e. the right branch in melt/accumulation

https://doi.org/10.5194/tc-2020-148
Preprint. Discussion started: 14 July 2020


conditions in Figs. 9e,f. When compared to the average for all years, it appears that indeed accumulation is significantly larger ($>1\sigma$) in April for efficient PFA formation. Melt is also slightly above this threshold, but not in a specific month. Apparently, total summer melt should just be large enough. It should be noted that this result is an average over multiple PFA locations, and suggests that PFA formation is a subtle process in which many factors, including the timing and seasonality of accumulation, play a role. This could be researched in more detail, specifically analyzing climatic regions, but this is beyond the scope of this exploratory study.

### 6.4 Ice shelves

Hydrofracturing has been implied in the breakup of Larsen A, Larsen B and Prince Gustav ice shelves (Scambos et al., 2000; Van den Broeke, 2005; Bell et al., 2018) as well as the recent breakup events of large parts of Wilkins ice shelf (Scambos et al., 2009). Ice-shelf breakup has typically been linked to meltwater ponding until it drains into surface crevasses, and subsurface water from PFAs might mitigate the potential of meltwater to reach ice shelves, and therewith the potential for hydrofracturing. A careful look at Figure 5 illustrates that, especially for SNOWPACK, PFA locations on grounded ice largely coincide with the grounding lines of ice shelves that have disappeared or are unstable, or with locations that have no ice shelf at all. The cases of Wordie and Wilkins ice shelves were discussed above, and especially the timing (late 90s) of PFAs on Wordie ice shelf coincides with some of its larger disintegration events (Cook et al., 2014). Other disintegrated ice shelves in the eastern AP, also show the potential for PFA presence on their grounding lines, e.g. former Prince Gustav and Larsen A ice shelves. This does not imply causation and could also simply be a result of warmer conditions resulting more melt, subsequent PFA formation. In future work, the potential role of PFAs on ice shelf stability will be studied in more detail.

## 7 Conclusions

Two snow models, the IMAU Firn Densification Model (IMAU-FDM) and SNOWPACK, are used to assess firn characteristics of Antarctic Peninsula (AP) glaciers, with a specific focus on predicting the presence of perennial firn aquifers (PFAs). PFAs represent surface meltwater that percolates into the firnpack in summer and remains liquid after being buried by snowfall during the following fall/winter. PFAs have the potential to slow down meltwater runoff into the ocean, or to impact ice shelf stability by modifying processes of ice shelf hydrofracturing and subsequent break-up. The two snow models are forced with with surface mass balance (SMB) and surface energy balance (SEB) output from the Regional Atmospheric Climate MOdel (RACMO2.3p2) at 5.5 km horizontal resolution, to construct a 1979–2016 climatology of AP firn density, temperature and liquid water content. A comparison with 75 snow temperature observations at 10 m depth and with density from 11 firn cores suggests that both snow models perform adequately. Both models tend to underestimate 10 m firn temperature (RMSD $=\sim$1.5K) but the spatial variability is represented well ($r^2$=0.90). SNOWPACK performs better in warmer locations with larger surface melt rates, which is important for the formation of PFAs. Both models tend to overestimate the amount of firn pore space, both in warm and cold locations, SNOWPACK more so as its dry densification rate is smaller. A comparison with liquid

https://doi.org/10.5194/tc-2020-148
Preprint. Discussion started: 14 July 2020


water content and PFA occurrences is not performed as accurate observations do not yet exist; previous studies have shown that both models are capable of simulating PFAs in Greenland (Steger et al., 2017a).

The two models predict 941 model grid cells, covering ∼28,000 $\mathrm{km}^2$, with a PFA that existed at least one year during 1979-2016. IMAU-FDM simulates 5% more PFAs than SNOWPACK, but generally the estimates of PFA locations are consistent among the models. PFAs are found in regions with both significant surface melt production and high accumulation rates. These conditions are met most frequently along the western coastline of the AP, but some smaller PFAs are also modelled on the eastern AP, notably near the grounding lines of former Prince Gustav, Larsen A and Larsen B ice shelves. The most extensive PFA system is modelled on the Wilkins ice shelf, which, in both models, is covered by PFAs over about 50% of its area. Towards the north, PFAs are predicted along the entire western AP coastline and on the adjacent islands, most significantly so in Palmer Land, where accumulation rates are often above 3000 $\mathrm{mm\ w.e.\ y}^{-1}$, i.e. highly efficient to isolate summer meltwater in the firn from the winter cold. Interannual variability of PFA presence is relatively large. Most PFAs exist longer than one year, several even during the whole 38 years of the model study, yet most PFAs are found in the period from 1987–2000, the warmest episode with enhanced melt rates. In the last two decades, PFA counts have significantly decreased, following the atmospheric cooling that has been reported for this period (Van Wessem et al., 2015; Turner et al., 2016).

Both increasing melt and accumulation rates generally favour PFA formation, but too much melt may result in a summer snowpack that melts away, and too much accumulation buries the meltwater so deep and adds so much cold content that the PFA never grows significantly. Optimal conditions for PFA formation, in which more than 50% of summer meltwater is retained in the subsequent winter, are found for melt/accumulation ratios of ∼0.1–0.2.

Not only the magnitude and ratio of yearly melt and accumulation are important, but also the seasonal variability. A relatively warm summer with high melt followed by a large accumulation event in the first months of fall (April) appears to favour PFA formation. On Wilkins ice shelf, PFAs are formed in many years, which, when large and deep enough, can merge deeper in the firn causing the PFA to grow. In northwest Palmer Land, a region with extremely large accumulation rates, deep aquifers are found but they seldom merge with firn aquifers of other years. For this to happen melt rates should be considerably larger.

This study is the first to model PFAs on Antarctica, and can help finding locations for observational-based studies on the potential of Antarctic PFAs. Additionally, it appears the location of most PFAs on the grounded ice coincide with grounding lines of (former) ice shelves that have disappeared or are disintegrating, such as Prince Gustav, Wilkins and Wordie ice shelves. Although this could be simply a coincidence of warmer locations, a further analysis will be performed to reveal to what extent PFAs impact ice shelf stability

## Acknowledgements

We are grateful for the financial support of NWO/ALW, Netherlands Polar Programme. This work was partly funded by the NWO (Netherlands Organisation for Scientific Research) VENI grant VI.Veni.192.083.

https://doi.org/10.5194/tc-2020-148
Preprint. Discussion started: 14 July 2020




## References

Alley, K. E., Scambos, T. A., Miller, J. Z., Long, D. G., and MacFerrin, M.: Quantifying vulnerability of Antarctic ice shelves to hydrofracture using microwave scattering properties, Remote Sensing of Environment, 210, 297–306, doi:10.1016/j.rse.2018.03.025, https://doi.org/10.1016/j.rse.2018.03.025, 2018.

Ashmore, D. W., Hubbard, B., Luckman, A., Kulessa, B., Bevan, S., Booth, A., Munneke, P. K., O'Leary, M., Sevestre, H., and Holland, P. R.: Ice and firn heterogeneity within Larsen C Ice Shelf from borehole optical televiewing, Journal of Geophysical Research: Earth Surface, 122, 1139–1153, doi:10.1002/2016JF004047, 2017.

Bartelt, P. and Lehning, M.: A physical SNOWPACK model for the Swiss avalanche warning: Part I: numerical model, Cold Regions Science and Technology, 35, 123–145, doi:https://doi.org/10.1016/S0165-232X(02)00074-5, http://www.sciencedirect.com/science/article/pii/S0165232X02000745, 2002.

Bell, R. E., Banwell, A. F., Trusel, L. D., and Kingslake, J.: Antarctic surface hydrology and impacts on ice-sheet mass balance, Nature Climate Change, doi:10.1038/s41558-018-0326-3, http://www.nature.com/articles/s41558-018-0326-3, 2018.

Brangers, I., Lievens, H., Miège, C., Demuzere, M., Brucker, L., and De Lannoy, G.: Sentinel-1 detects firn aquifers in the Greenland Ice Sheet, Geophysical Research Letters, doi:10.1029/2019gl085192, 2020.

Bromwich, D. H., Nicolas, J. P., Hines, K. M., Kay, J. E., Key, E. L., Lazzara, M. A., Lubin, D., Mcfarquhar, G. M., Gorodetskaya, I. V., Grosvenor, D. P., Cope, T. L., and Lipzig, N. P. M. V.: Tropospheric Clouds in Antarctica, Reviews of Geophysics, 50, 1–40, doi:10.1029/2011RG000363.1.INTRODUCTION, 2012.

Cook, A. J., Vaughan, D. G., Luckman, A. J., and Murray, T.: A new Antarctic Peninsula glacier basin inventory and observed area changes since the 1940s, Antarctic Science, 26, 614–624, doi:10.1017/S0954102014000200, http://www.journals.cambridge.org/abstract{_}S0954102014000200, 2014.

Cook, A. J., Holland, P. R., Meredith, M. P., Murray, T., Luckman, A., Vaughan, D. G., Huss, M., Farinotti, D., Marshall, G. J., Orr, A., van Lipzig, N. P. M., King, J. C., Kunz, M., King, M. A., Mills, J. P., Miller, P. E., Fox, A. J., Vaughan, D. G., Marsh, S. H., Barrand, N. E., Vaughan, D. G., Steiner, N., Tedesco, M., Munneke, P. K., van den Broeke, M. R., Hosking, J. S., Holland, P., Brisbourne, A., Corr, H. F. J., McGrath, D., Purdon, K., Paden, J., Fricker, H. A., Paolo, F. S., Fleming, A. H., Pritchard, H. D., Vaughan, D. G., Cook, A. J., Vaughan, D. G., Luckman, A., Murray, T., Cook, A. J., Fox, A. J., Vaughan, D. G., Ferrigno, J. G., Comiso, J. C., van Wessem, J. M., Ligtenberg, S. R. M., Reijmer, C. H., van de Berg, W. J., van den Broeke, M. R., Barrand, N. E., Thomas, E. R., Turner, J., Wuite, J., Scambos, T. A., van Meijgaard, E., Paolo, F. S., Fricker, H. A., Padman, L., Wouters, B., Martin-EspaÑol, A., Helm, V., Flament, T., van Wessem, J. M., Ligtenberg, S. R., van den Broeke, M. R., Bamber, J. L., Holland, P. R., Jenkins, A., Holland, D. M., Pritchard, H. D., Ligtenberg, S. R., Fricker, H. A., Vaughan, D. G., van den Broeke, M. R., Padman, L., Shepherd, A., Wingham, D. J., Rignot, E., Dutrieux, P., Rydt, J. D., Jenkins, A., Holland, P. R., Ha, H. K., Lee, S. H., Steig, E. J., Ding, Q., Abrahamsen, E. P., Schröder, M., Luckman, A., Benn, D. I., Cottier, F., Bevan, S., Nilsen, F., Inall, M., Whitworth, T., Nowlin, W., Orsi, A., Locarnini, R., Smith, S., Holland, P. R., Jenkins, A., Holland, D. M., Jenkins, A., Greisman, P., Motyka, R. J., Hunter, L., Echelmeyer, K. A., Connor, C., Straneo, F., Curry, R. G., Sutherland, D. A., Hamilton, G. S., Cenedese, C., Våge, K., Stearns, L. A., Dotto, T. S., Kerr, R., Mata, M. M., Garcia, C. A., Martinson, D. G., Stammerjohn, S. E., Iannuzzi, R. A., Smith, R. C., Vernet, M., Schmidtko, S., Heywood, K. J., Thompson, A. F., Aoki, S., Padman, L., Costa, D. P., Dinniman, M. S., Fricker, H. A., Goebel, M. E., Huckstadt, L. A., Humbert, A., Joughin, I., Lenaerts, J. T. M., Ligtenberg, S. R. M., Scambos, T., van den Broeke, M. R., Arndt, J. E., Schenke, H. W., Jakobsson, M., Nitsche, F. O., Buys, G., Goleby, B., Rebesco,

https://doi.org/10.5194/tc-2020-148
Preprint. Discussion started: 14 July 2020




M., Bohoyo, F., Hong, J., Black, J., Greku, R., Udintsev, G., Barrios, F., Reynoso-Peralta, W., Taisei, M., and Wigley, R.: Ocean forcing of glacier retreat in the western Antarctic Peninsula, Science, 353, 1261–1273, doi:10.1126/science.aae0017, 2016.

Ettema, J., Van den Broeke, M. R., Van Meijgaard, E., Van de Berg, W. J., Box, J. E., and Steffen, K.: Climate of the Greenland ice sheet using a high-resolution climate model – Part 1: Evaluation, The Cryosphere, 4, 529–544, doi:10.5194/tc-4-511-2010, http://www.the-cryosphere.net/4/529/2010/http://www.the-cryosphere.net/4/511/2010/, 2010.

Forster, R. R., Box, J. E., van den Broeke, M. R., Miège, C., Burgess, E. W., van Angelen, J. H., Lenaerts, J. T. M., Koenig, L. S., Paden, J., Lewis, C., Gogineni, S. P., Leuschen, C., and McConnell, J. R.: Extensive liquid meltwater storage in firn within the Greenland ice sheet, Nature Geoscience, 7, 95–98, doi:10.1038/ngeo2043, http://www.nature.com/doifinder/10.1038/ngeo2043, 2013.

Holland, P. R., Corr, H. F. J., Pritchard, H. D., Vaughan, D. G., Arthern, R. J., Jenkins, A., and Tedesco, M.: The air content of Larsen Ice Shelf, Geophysical Research Letters, 38, n/a–n/a, doi:10.1029/2011GL047245, http://doi.wiley.com/10.1029/2011GL047245, 2011.

Hubbard, B., Luckman, A., Ashmore, D. W., Bevan, S., Kulessa, B., Munneke, P. K., Philippe, M., Jansen, D., Booth, A., Sevestre, H., Tison, J.-L., O'Leary, M., and Rutt, I.: Massive subsurface ice formed by refreezing of ice-shelf melt ponds, Nature Communications, 7, 1–6, doi:10.1038/ncomms11897, 2016.

Jakobs, C. L., Reijmer, C. H., Munneke, P. K., König-langlo, G., Broeke, R. V. D., Kuipers Munneke, P., König-langlo, G., and Van Den Broeke, M. R.: Quantifying the snowmelt-albedo feedback at Neumayer Station, East Antarctica, The Cryosphere Discussions, 2018, 1–31, doi:10.5194/tc-2018-221, https://www.the-cryosphere-discuss.net/tc-2018-221/, 2018.

Kingslake, J., Ely, J. C., Das, I., and Bell, R. E.: Widespread movement of meltwater onto and across Antarctic ice shelves, Nature, 544, 349–352, doi:10.1038/nature22049, http://dx.doi.org/10.1038/nature22049, 2017.

Kuipers Munneke, P., Van den Broeke, M. R., Lenaerts, J. T. M., Flanner, M. G., Gardner, A. S., and Van de Berg, W. J.: A new albedo parameterization for use in climate models over the Antarctic ice sheet, Journal of Geophysical Research, 116, 1–10, doi:10.1029/2010JD015113, http://www.agu.org/pubs/crossref/2011/2010JD015113.shtml, 2011.

Kuipers Munneke, P., Ligtenberg, S. R. M., Van den Broeke, M. R., Van Angelen, J. H., and Forster, R. R.: Explaining the presence of perennial liquid water bodies in the firn of the Greenland Ice Sheet, Geophysical Research Letters, pp. 476–483, doi:10.1002/2013GL058389.1., 2014a.

Kuipers Munneke, P., Ligtenberg, S. R. M., Van Den Broeke, M. R., and Vaughan, D. G.: Firn air depletion as a precursor of Antarctic ice-shelf collapse, Journal of Glaciology, 60, 205–214, doi:10.3189/2014JoG13J183, http://www.igsoc.org/journal/60/220/t13J183.html, 2014b.

Kuipers Munneke, P., Luckman, A. J., Bevan, S. L., Gilbert, E., Smeets, C. J. P. P., van den Broeke, M. R., Gilbert, E., van den Broeke, M. R., Wang, W., Zender, C., Hubbard, B., Ashmore, D., Orr, A., King, J. C., and Kulessa, B.: Intense winter surface melt on an Antarctic ice shelf, In preparation, 45, 1–18, doi:10.1029/2018GL077899, 2018.

Lehning, M., Bartelt, P., Brown, B., Fierz, C., and Satyawali, P.: A physical SNOWPACK model for the Swiss avalanche warning Part II. Snow microstructure, Cold Regions Science and Technology, 35, 147–167, doi:10.1016/S0165-232X(02)00073-3, 2002.

Lehning, M., Völksch, I., Gustafsson, D., Nguyen, T. A., Stähli, M., and Zappa, M.: ALPINE3D: a detailed model of mountain surface processes and its application to snow hydrology, Hydrological Processes: An International Journal, 20, 2111–2128, 2006.

Lenaerts, J. T. M., van den Broeke, M. R., Déry, S. J., Van Meijgaard, E., Van de Berg, W. J., Palm, S. P., and Sanz Rodrigo, J.: Modeling drifting snow in Antarctica with a regional climate model: 1. Methods and model evaluation, Journal of Geophysical Research, 117, 1–11, doi:10.1029/2011JD016145, http://www.agu.org/pubs/crossref/2012/2011JD016145.shtmlhttp://doi.wiley.com/10.1029/2011JD016145http://www.agu.org/pubs/crossref/2012/2010JD015419.shtml, 2012.

https://doi.org/10.5194/tc-2020-148
Preprint. Discussion started: 14 July 2020


Lenaerts, J. T. M., Lhermitte, S., Drews, R., Ligtenberg, S. S., Berger, S., Helm, V., Smeets, C. C., Broeke, M. M., Van de Berg, W., Van Meijgaard, E., Eijkelboom, M., Eisen, O., Pattyn, F., van de Berg, W., van Meijgaard, E., Eijkelboom, M., Eisen, O., and Pattyn, F.: Meltwater produced by wind-albedo interaction stored in an East Antarctic ice shelf, Nature Climate Change, 7, 58–62, doi:10.1038/nclimate3180, http://www.nature.com/doifinder/10.1038/nclimate3180, 2016.

Ligtenberg, S. R. M., Helsen, M. M., and van den Broeke, M. R.: An improved semi-empirical model for the densification of Antarctic firn, The Cryosphere, 5, 809–819, doi:10.5194/tc-5-809-2011, http://www.the-cryosphere.net/5/809/2011/, 2011.

Ligtenberg, S. R. M., Kuipers Munneke, P., Noël, B. P. Y., and van den Broeke, M. R.: Brief communication: Improved simulation of the present-day Greenland firn layer (1960–2016), The Cryosphere Discussions, pp. 1–10, doi:10.5194/tc-2017-282, https://www.the-cryosphere-discuss.net/tc-2017-282/, 2018.

Montgomery, L., Koenig, L., and Alexander, P.: The SUMup dataset: Compiled measurements of surface mass balance components over ice sheets and sea ice with analysis over Greenland, Earth System Science Data, 10, 1959–1985, doi:10.5194/essd-10-1959-2018, 2018.

Morris, E. M. and Vaughan, D. G.: Spatial and temporal variation of surface temperature on the Antarctic Peninsula and the limit of viability of ice shelves, Antarctic Research Series, 79, 61–68, 2003.

Munneke, P. K., McGrath, D., Medley, B., Luckman, A., Bevan, S., Kulessa, B., Jansen, D., Booth, A., Smeets, P., Hubbard, B., Ashmore, D., Van den Broeke, M., Sevestre, H., Steffen, K., Shepherd, A., Gourmelen, N., Kuipers Munneke, P., McGrath, D., Medley, B., Luckman, A., Bevan, S., Kulessa, B., Jansen, D., Booth, A., Smeets, P., Hubbard, B., Ashmore, D., Van den Broeke, M., Sevestre, H., Steffen, K., Shepherd, A., and Gourmelen, N.: Observationally constrained surface mass balance of Larsen C Ice Shelf, Antarctica, The Cryosphere, 11, 1–24, doi:10.5194/tc-2017-44, http://www.the-cryosphere-discuss.net/tc-2017-44/, 2017.

Reijmer, C. H., van den Broeke, M. R., Fettweis, X., Ettema, J., and Stap, L. B.: Refreezing on the Greenland ice sheet: a comparison of parameterizations, The Cryosphere, 6, 743–762, doi:10.5194/tc-6-743-2012, http://www.the-cryosphere.net/6/743/2012/, 2012.

Scambos, T., Fricker, H. A., Liu, C.-C., Bohlander, J., Fastook, J., Sargent, A., Massom, R., and Wu, A.-M.: Ice shelf disintegration by plate bending and hydro-fracture: Satellite observations and model results of the 2008 Wilkins ice shelf break-ups, Earth and Planetary Science Letters, 280, 51–60, doi:10.1016/j.epsl.2008.12.027, http://linkinghub.elsevier.com/retrieve/pii/S0012821X08007887, 2009.

Scambos, T. A., Hulbe, C., Fahnestock, M., and Bohlander, J.: The link between climate warming and break-up of ice shelves in the Antarctic Peninsula, Journal of Glaciology, 46, 516–530, doi:10.3189/172756500781833043, http://openurl.ingenta.com/content/xref?genre=article{&}issn=0022-1430{&}volume=46{&}issue=154{&}spage=516, 2000.

Schmidtko, S., Heywood, K. J., Thompson, A. F., and Aoki, S.: Multidecadal warming of Antarctic waters., Science (New York, N.Y.), 346, 1227–31, doi:10.1126/science.1256117, http://www.sciencemag.org/content/346/6214/1227.short, 2014.

Stammerjohn, S., Maksym, T., Heil, P., Massom, R. A., Vancoppenolle, M., and Leonard, K. C.: The influence of winds, sea-surface temperature and precipitation anomalies on Antarctic regional sea-ice conditions during IPY 2007, Deep Sea Research Part II: Topical Studies in Oceanography, 58, 999–1018, doi:10.1016/j.dsr2.2010.10.026, http://www.sciencedirect.com/science/article/pii/S0967064510003048, 2011.

Steger, C. R., Reijmer, C. H., and van den Broeke, M. R.: The modelled liquid water balance of the Greenland Ice Sheet, The Cryosphere, pp. 1–32, doi:10.5194/tc-2017-88, 2017a.

Steger, C. R., Reijmer, C. H., van den Broeke, M. R., Wever, N., Forster, R. R., Koenig, L. S., Kuipers Munneke, P., Lehning, M., Lhermitte, S., Ligtenberg, S. R. M., Miège, C., and Noël, B. P. Y.: Firn Meltwater Retention on the Greenland Ice Sheet: A Model Comparison, Frontiers in Earth Science, 5, doi:10.3389/feart.2017.00003, http://journal.frontiersin.org/article/10.3389/feart.2017.00003/full, 2017b.

https://doi.org/10.5194/tc-2020-148
Preprint. Discussion started: 14 July 2020




Thomas, E. R., Marshall, G. J., and McConnell, J. R.: A doubling in snow accumulation in the western Antarctic Peninsula since 1850, Geophysical Research Letters, 35, 1–5, doi:10.1029/2007GL032529, http://www.agu.org/pubs/crossref/2008/2007GL032529.shtml, 2008.

Turner, J., Lu, H., White, I., King, J. C., Phillips, T., Hosking, J. S., Bracegirdle, T. J., Marshall, G. J., Mulvaney, R., and Deb, P.: Absence of 21st century warming on Antarctic Peninsula consistent with natural variability, Nature, 535, 411–415, doi:10.1038/nature18645, http://www.nature.com/doifinder/10.1038/nature18645, 2016.

Undén, P., Rontu, L., Jarvinen, H., Lynch, P., Calvo, J., Cats, G., Cuxart, J., Eerola, K., Fortelius, C., Garcia-moya, J., Jones, C., Lenderlink, G., Mcdonald, A., Mcgrath, R., and Navascues, B.: HIRLAM-5 Scientific Documentation, Tech. Rep. December, Swedish Meteorology and Hydrology Institute, 2002.

van Dalum, C. T., van de Berg, W. J., Libois, Q., Picard, G., and van den Broeke, M. R.: A module to convert spectral to narrowband snow albedo for use in climate models: SNOWBAL v1.0, Geoscientific Model Development Discussions, 2018, 1–26, doi:10.5194/gmd-2018-175, https://www.geosci-model-dev-discuss.net/gmd-2018-175/, 2018.

Van den Broeke, M. R.: Strong surface melting preceded collapse of Antarctic Peninsula ice shelf, Geophysical Research Letters, 32, 2–5, doi:10.1029/2005GL023247, http://www.agu.org/pubs/crossref/2005/2005GL023247.shtml, 2005.

Van Wessem, J. M., Reijmer, C. H., Van de Berg, W. J., Van den Broeke, M. R., Cook, A. J., Van Ulft, L. H., and Van Meijgaard, E.: Temperature and Wind Climate of the Antarctic Peninsula as Simulated by a High-Resolution Regional Atmospheric Climate Model, Journal of Climate, 28, 7306–7326, doi:10.1175/JCLI-D-15-0060.1, http://journals.ametsoc.org/doi/abs/10.1175/JCLI-D-15-0060.1, 2015.

Van Wessem, J. M., Ligtenberg, S. R. M., Reijmer, C. H., van de Berg, W. J., van den Broeke, M. R., Barrand, N. E., Thomas, E. R., Turner, J., Wuite, J., Scambos, T. A., and van Meijgaard, E.: The modelled surface mass balance of the Antarctic Peninsula at 5.5 km horizontal resolution, The Cryosphere, 10, 271–285, doi:10.5194/tc-10-271-2016, 2016.

Van Wessem, J. M., van de Berg, W. J., Noël, B. P. Y., van Meijgaard, E., Birnbaum, G., Jakobs, C. L., Krüger, K., Lenaerts, J. T. M., Lhermitte, S., Ligtenberg, S. R. M., Medley, B., Reijmer, C. H., van Tricht, K., Trusel, L. D., van Ulft, L. H., Wouters, B., Wuite, J., Amory, C., and van den Broeke, M. R.: Modelling the climate and surface mass balance of polar ice sheets using RACMO2, part 2: Antarctica (1979–2016), The Cryosphere, 2018, 1–35, doi:10.5194/tc-2017-202, 2018.

Wever, N., Würzer, S., Fierz, C., and Lehning, M.: Simulating ice layer formation under the presence of preferential flow in layered snowpacks, Cryosphere, 10, 2731–2744, doi:10.5194/tc-10-2731-2016, 2016.

https://doi.org/10.5194/tc-2020-148
Preprint. Discussion started: 14 July 2020


The Cryosphere Discussions
Open Access
EGU

**Table 1.** Density from 11 firn cores used for comparison with modelled firn density. See Munneke et al. (2017) for details of the shallow cores (upper six) and Ashmore et al. (2017) for the deeper cores.

| Site | Latitude | Longitude | Depth (m) |
|---|---|---|---|
| J1_08 | 67.1 | 61.3 | 30 |
| J2_08 | 68.3 | 68.15 | 30 |
| J4_08 | 68.4 | 64.7 | 30 |
| LAR1 | 68.14 | 63.95 | 6 |
| LAR2 | 67.57 | 63.25 | 5 |
| LAR3 | 67.03 | 62.64 | 5 |
| CI-0 | -66.4 | -63.38 | 97.5 |
| CI-22 | -66.6 | -63.2 | 90 |
| CI-120 | -67.0 | -61.5 | 90 |
| WI 0 | -67.4 | -64.9 | 90 |
| WI 70 | -67.5 | -63.3 | 90 |

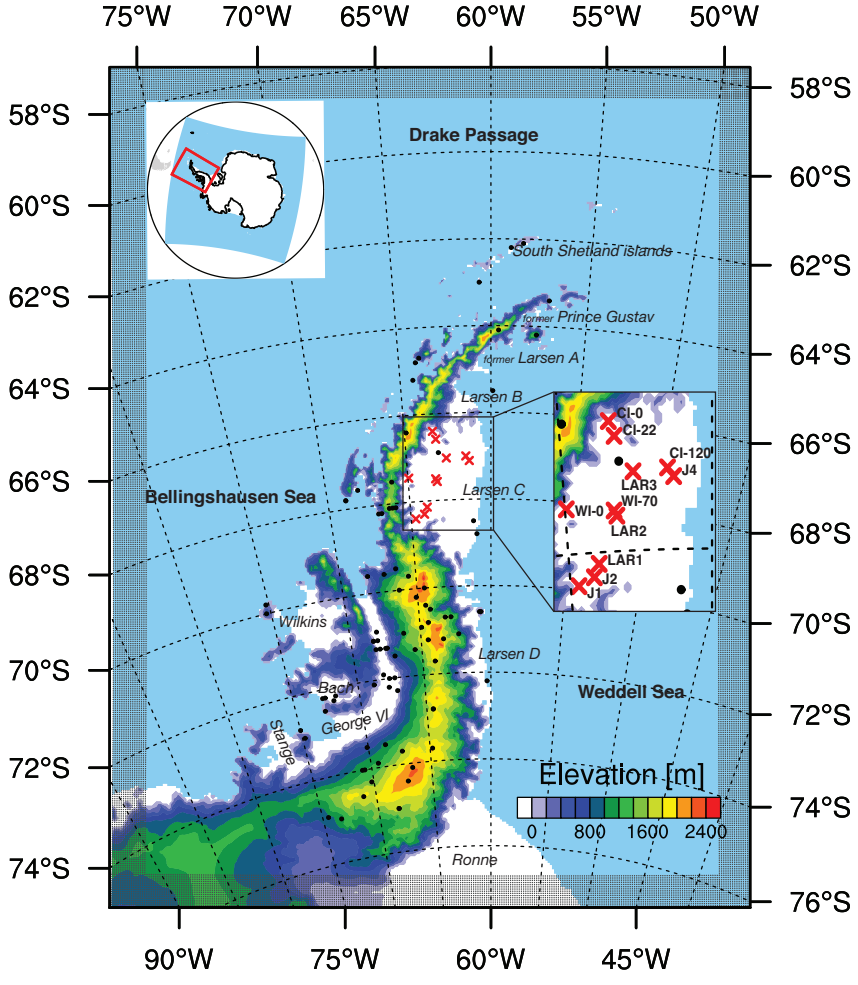


**Figure 1.** RACMO2 model domain (red box in inset map of Antarctica) and surface topography (m) of the Antarctic Peninsula. Locations of 10 m snow temperature observations are marked (black dots), as well as the density profiles (red crosses). Model topography is based on digital elevation models described in Van Wessem et al. (2018). White areas represent the floating ice shelves, coloured contours represent the grounded ice sheet.

https://doi.org/10.5194/tc-2020-148
Preprint. Discussion started: 14 July 2020


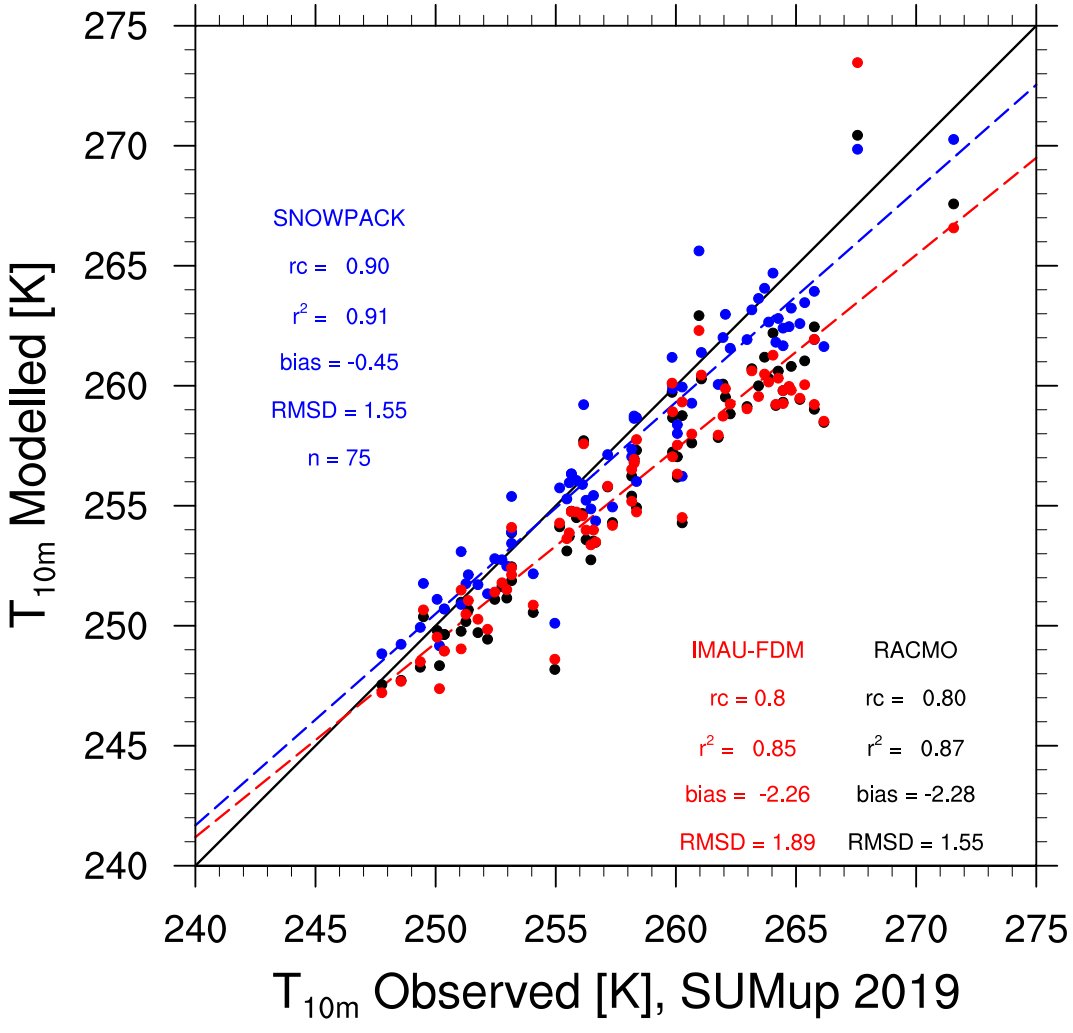


**Figure 2.** Modelled IMAU-FDM (red), SNOWPACK (blue) and RACMO (black) 10 m snow temperature as a function of observed 10 m snow temperature. Modelled temperature is corrected for discrepancies in elevation using a lapse rate of 7.2 K $\mathrm{km}^{-1}$. Statistics (slope (rc), $r^2$, bias and RMSD) for SNOWPACK, IMAU-FDM and RACMO-FDM are denoted based on all 75 locations. Observations are from Montgomery et al. (2018) and selected as described in Section 2.4.1.

https://doi.org/10.5194/tc-2020-148
Preprint. Discussion started: 14 July 2020


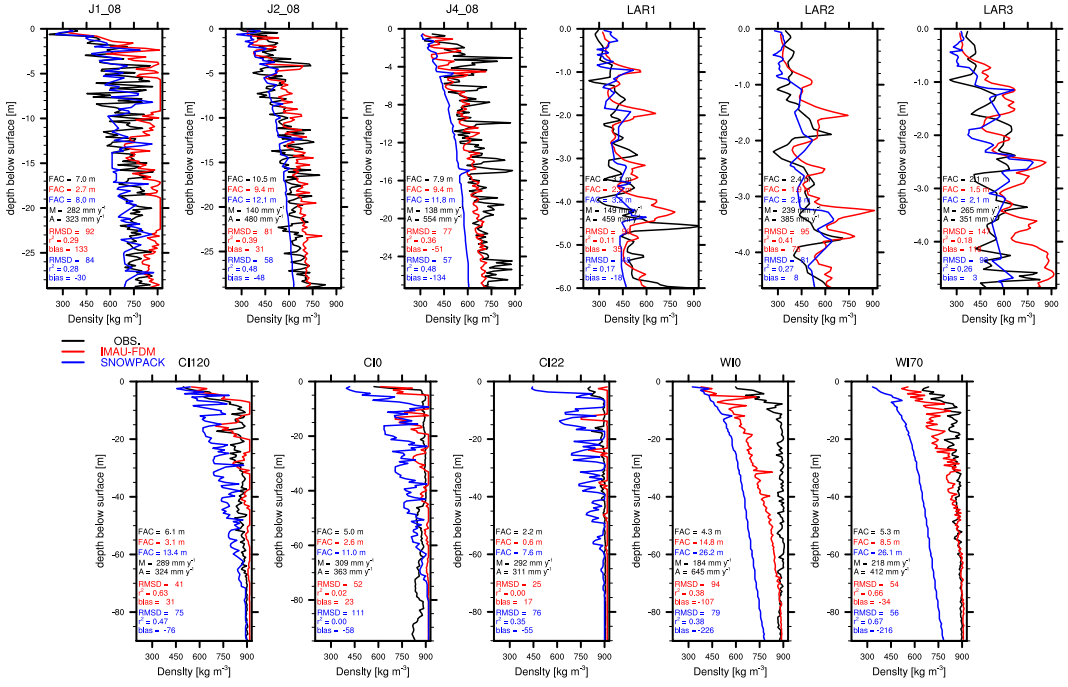


**Figure 3.** Modelled IMAU-FDM (red), SNOWPACK (blue) and observed (black) density profiles for 11 locations on the Larsen C ice shelf (Sect. 2.4.2). Denoted are vertical averaged Firn Air Content (FAC), annual average surface melt (M) and accumulation (A), $r^2$, bias and RMSD.

https://doi.org/10.5194/tc-2020-148
Preprint. Discussion started: 14 July 2020


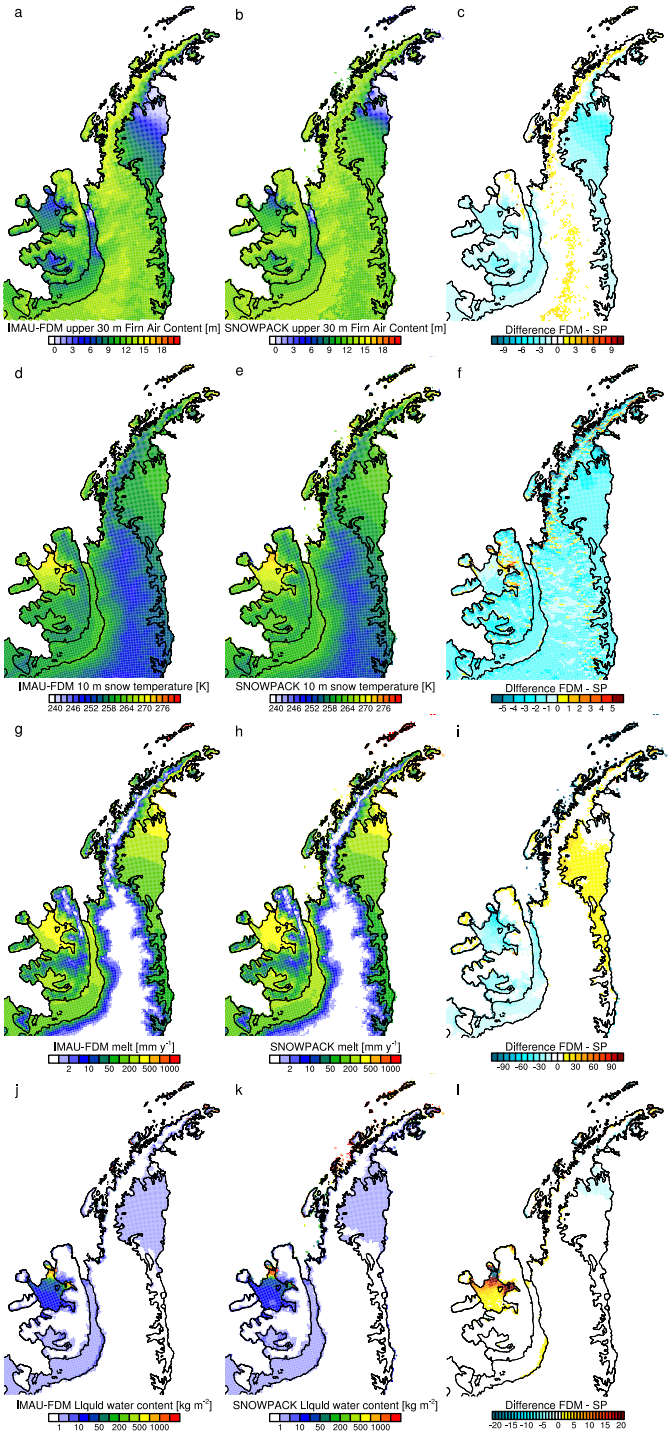


**Figure 4.** Modelled IMAU-FDM (left column), SNOWPACK (middle column) and their difference (IMAU-FDM - SNOWPACK) (right column) annual average (1979–2016) (a-c) Firn Air Content (FAC; m), (d-f) 10 m snow temperature (K), (g-i) surface meltwater production ($\mathrm{mm\ w.e.\ y^{-1}}$) and (j-l) vertically integrated liquid water content ($\mathrm{kg\ m^{-2}}$).

https://doi.org/10.5194/tc-2020-148
Preprint. Discussion started: 14 July 2020


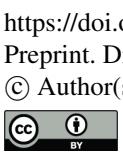

The Cryosphere
Discussions
Open Access
EGU

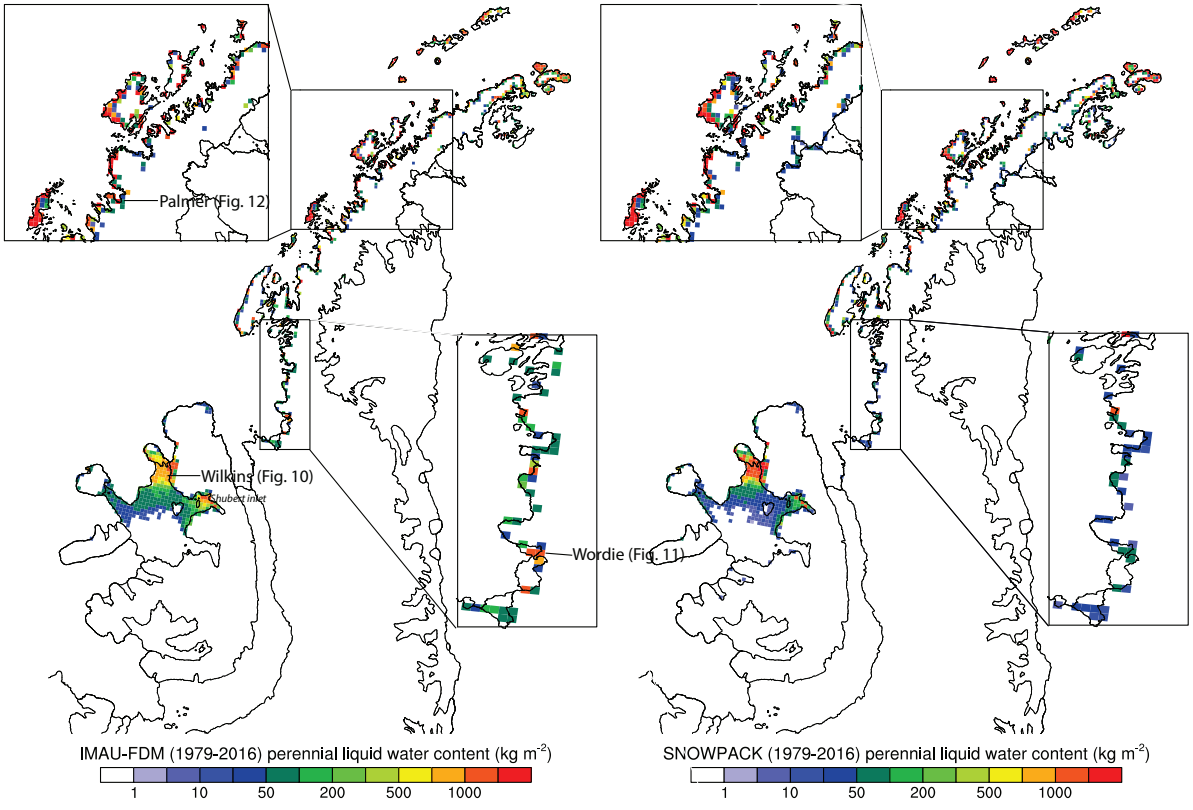


**Figure 5.** Modelled IMAU-FDM (left row) and SNOWPACK (right row) annual average (1979–2016) vertically integrated liquid water content for PFA points, see text.

https://doi.org/10.5194/tc-2020-148
Preprint. Discussion started: 14 July 2020


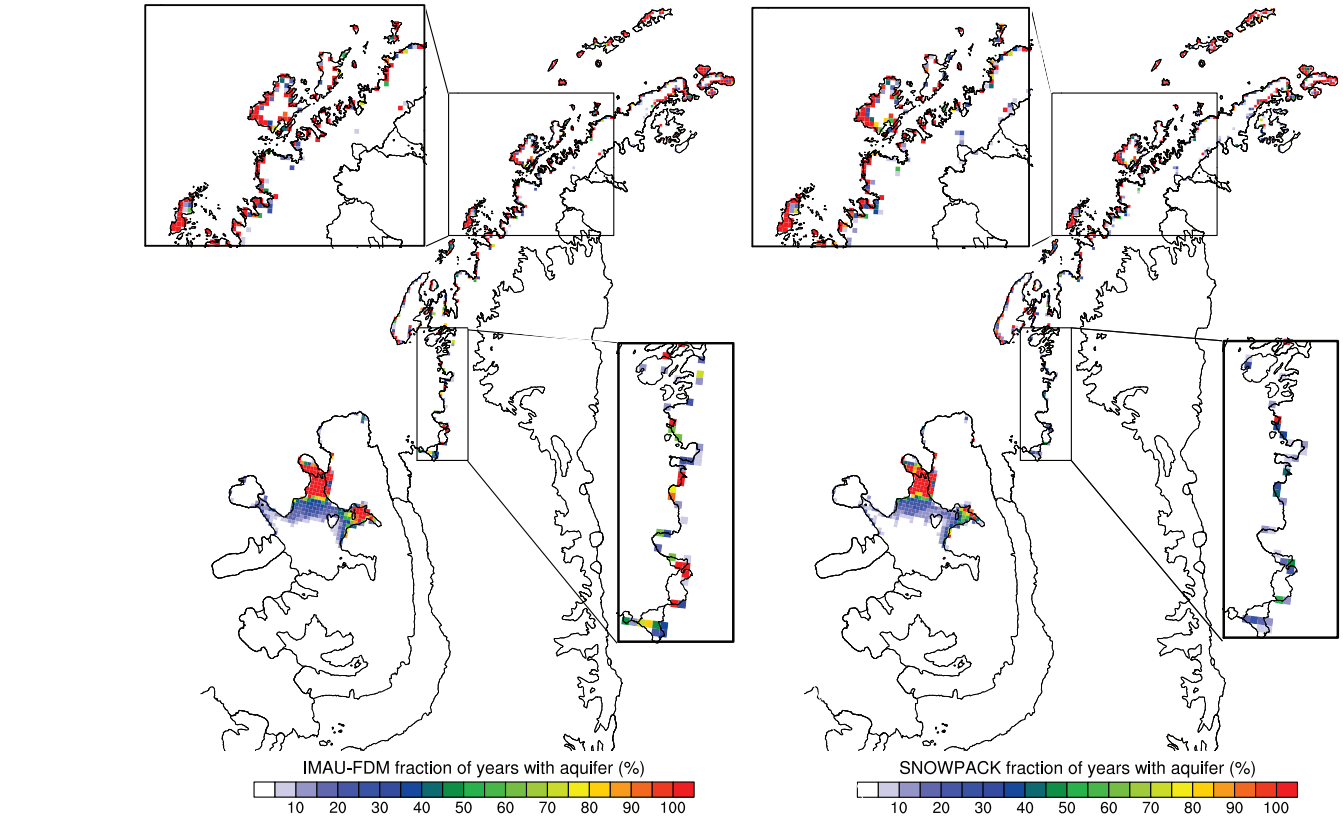


**Figure 6.** Modelled IMAU-FDM (left row) and SNOWPACK (right row) percentage of total years from 1979–2016 with vertically integrated liquid water liquid water for PFA points, see text.

https://doi.org/10.5194/tc-2020-148
Preprint. Discussion started: 14 July 2020


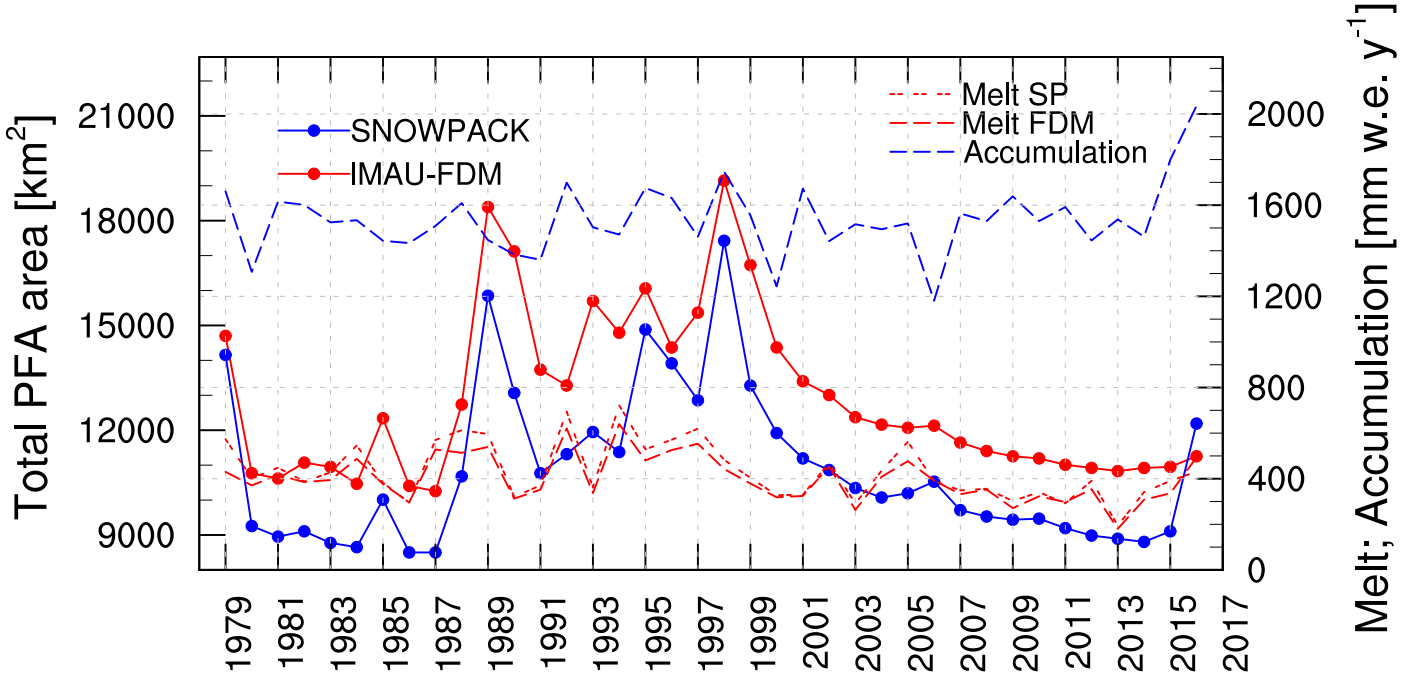


**Figure 7.** Yearly area of PFAs for SNOWPACK (blue solid line) and IMAU-FDM (red solid line) on the left axis, and yearly accumulation (blue dashed line) and melt (red dashed lines) averaged over all 941 PFA locations.

https://doi.org/10.5194/tc-2020-148
Preprint. Discussion started: 14 July 2020


The Cryosphere
Discussions
Open Access
EGU

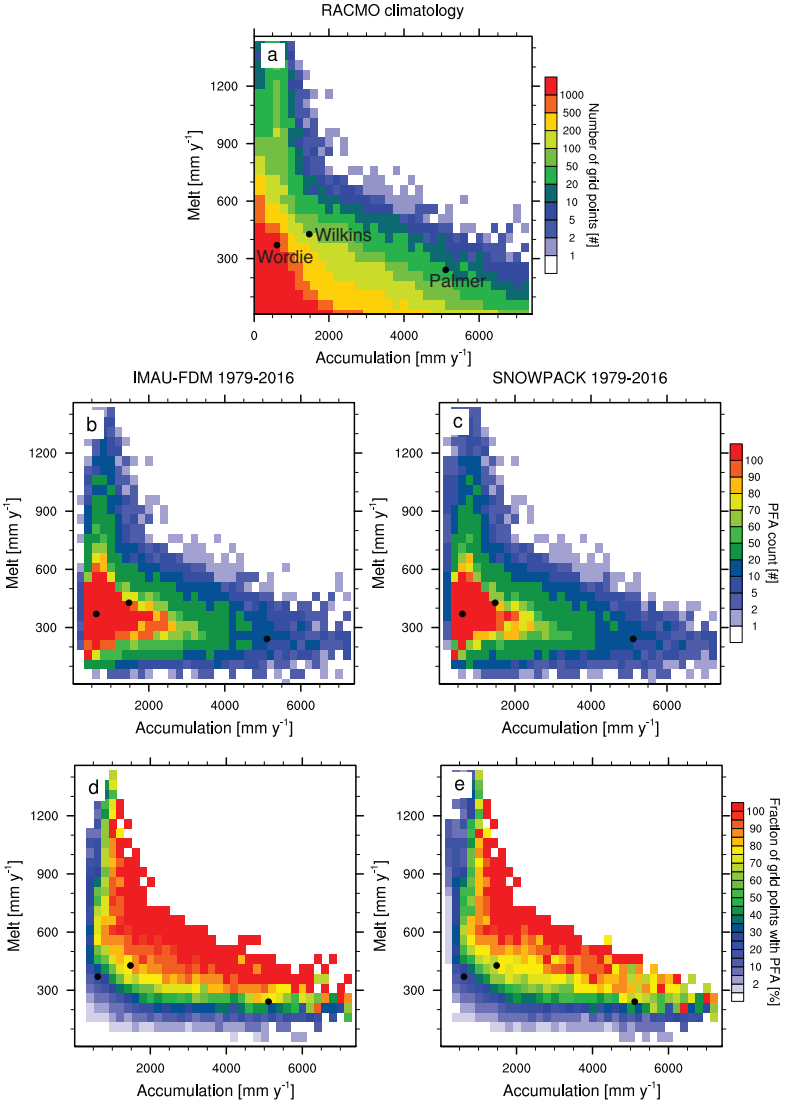


**Figure 8.** (a) Total number of model grid points, (b,c) total number of PFA occurrences for all model grid points in the respective hydrological year of the PFA , (d,e) percentage of total number of PFA occurrences in (d,e), as a function of yearly surface meltwater production (y-axis) and accumulation (x-axis). PFA numbers are binned in 50 $\mathrm{mm\ w.e.\ y^{-1}}$ intervals in the y-direction and by 200 $\mathrm{mm\ w.e.\ y^{-1}}$ in the x-direction. Grid points with only one occurrence are not shown.

https://doi.org/10.5194/tc-2020-148
Preprint. Discussion started: 14 July 2020


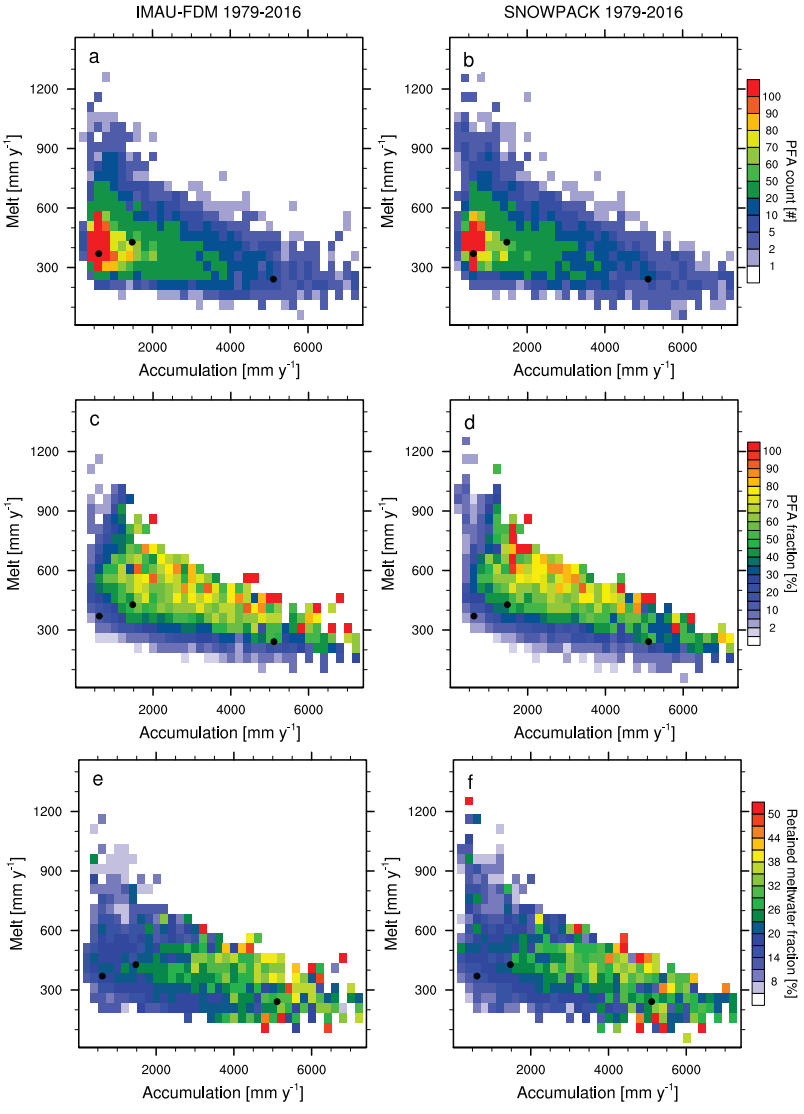


**Figure 9.** (a,b) Total number of PFA occurrences of (increases in) perennial firn liquid water for all model grid points in the respective hydrological year of the PFA , (c,d) percentage of total number of PFA occurrences (w.r.t. Fig. 8a and (e,f), percentage of total produced meltwater that is retained in the firn at the end of the subsequent winter, as a function of yearly surface meltwater production (y-axis) and accumulation (x-axis). PFA numbers are binned in 50 $\mathrm{mm\ w.e.\ y^{-1}}$ intervals in the y-direction and by 200 $\mathrm{mm\ w.e.\ y^{-1}}$ in the x-direction. Grid points with only one occurrence are not shown.

https://doi.org/10.5194/tc-2020-148
Preprint. Discussion started: 14 July 2020


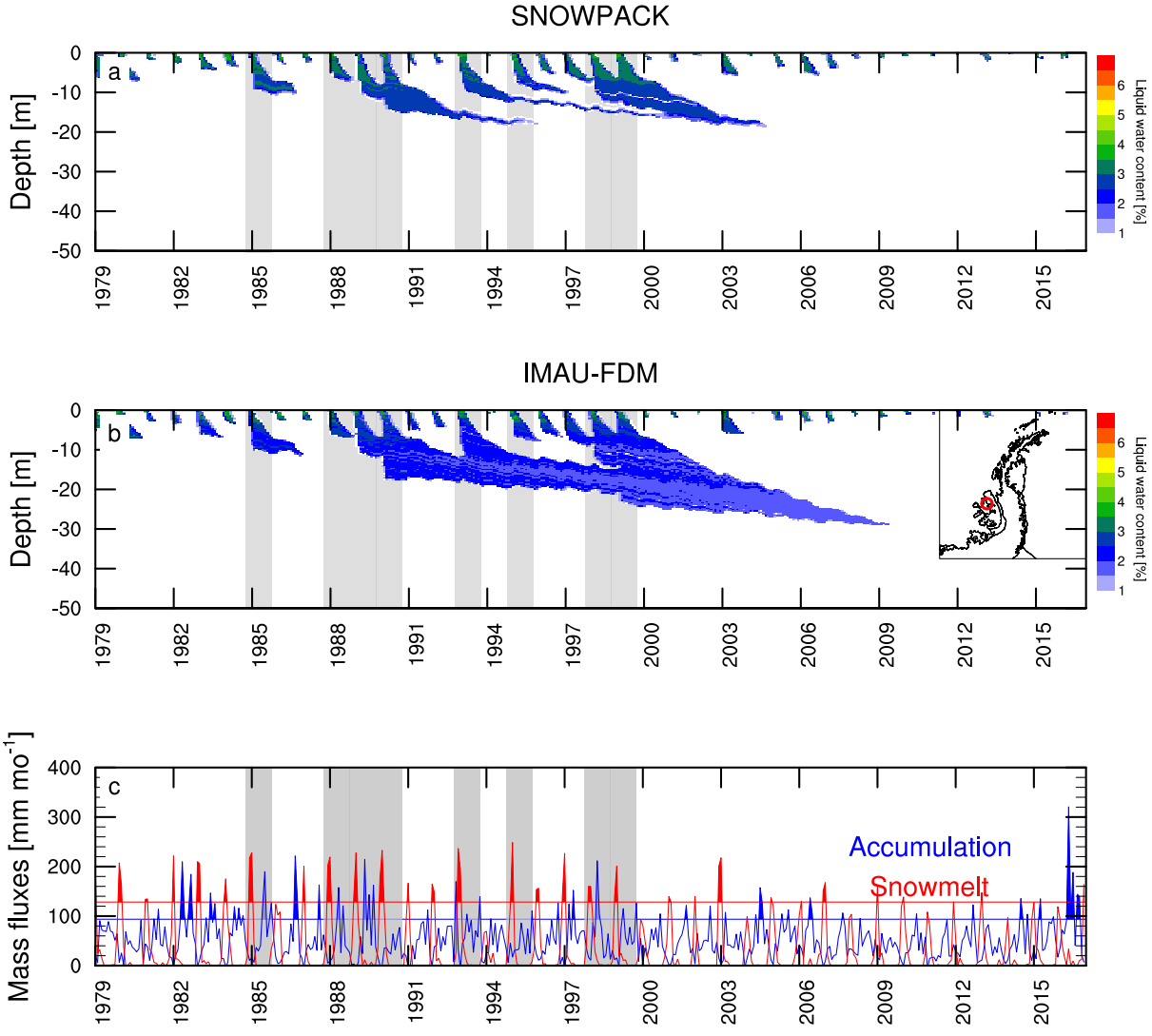


**Figure 10.** Volumetric water content for SNOWPACK (a) and IMAU-FDM (b) for 1979–2016 at a location on Wilkins ice shelf (see inset and Fig. 5). c) Monthly accumulation (blue) and surface melt production (red) for the same location; both horizontal lines note the mean + one standard deviation ($\sigma$) threshold. Grey bars denote hydrological years in which >5% of meltwater is retained.

https://doi.org/10.5194/tc-2020-148
Preprint. Discussion started: 14 July 2020


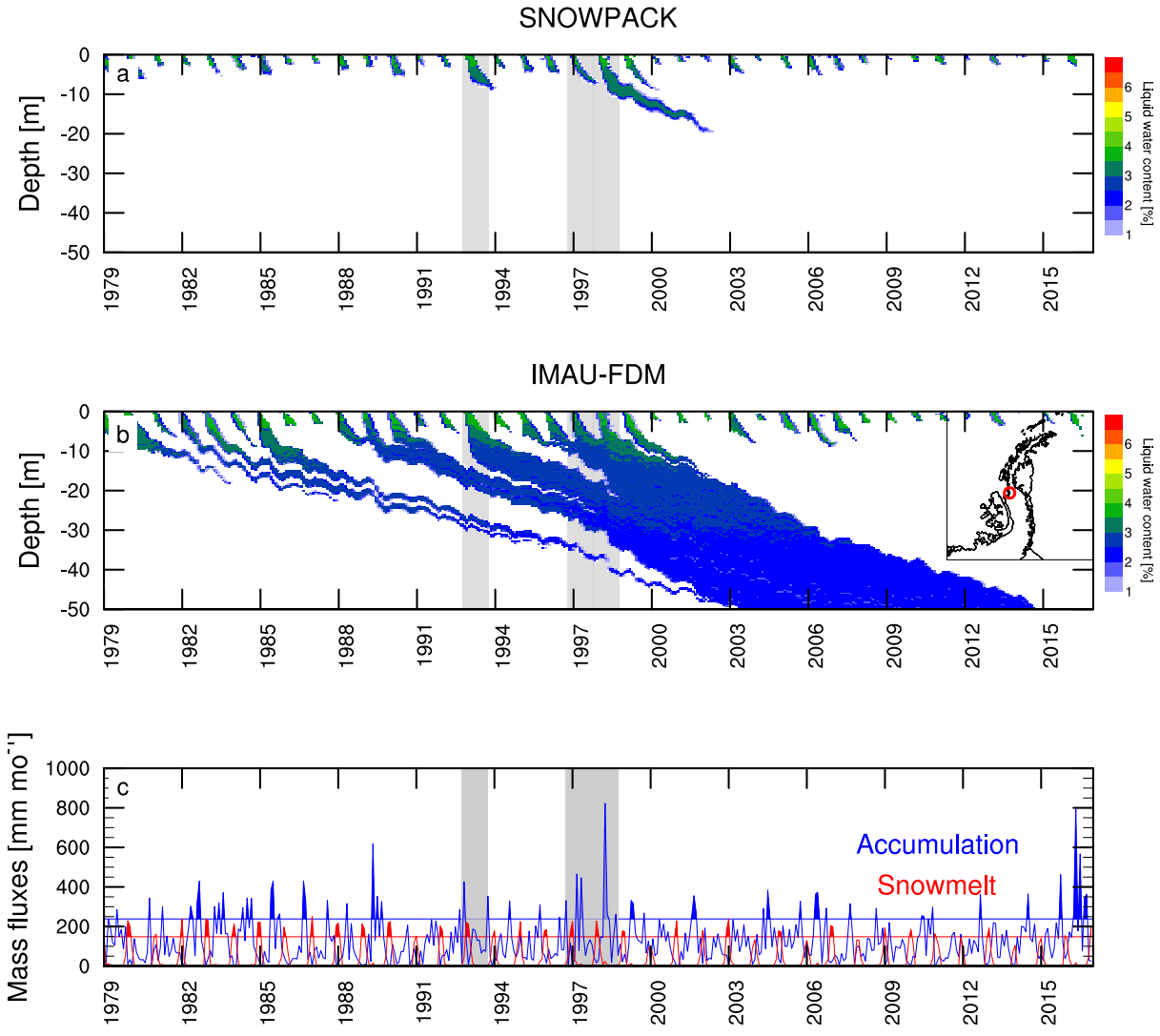


**Figure 11.** As for Fig. 9 but for a location on Wordie ice shelf (see inset and Fig. 5).

https://doi.org/10.5194/tc-2020-148
Preprint. Discussion started: 14 July 2020


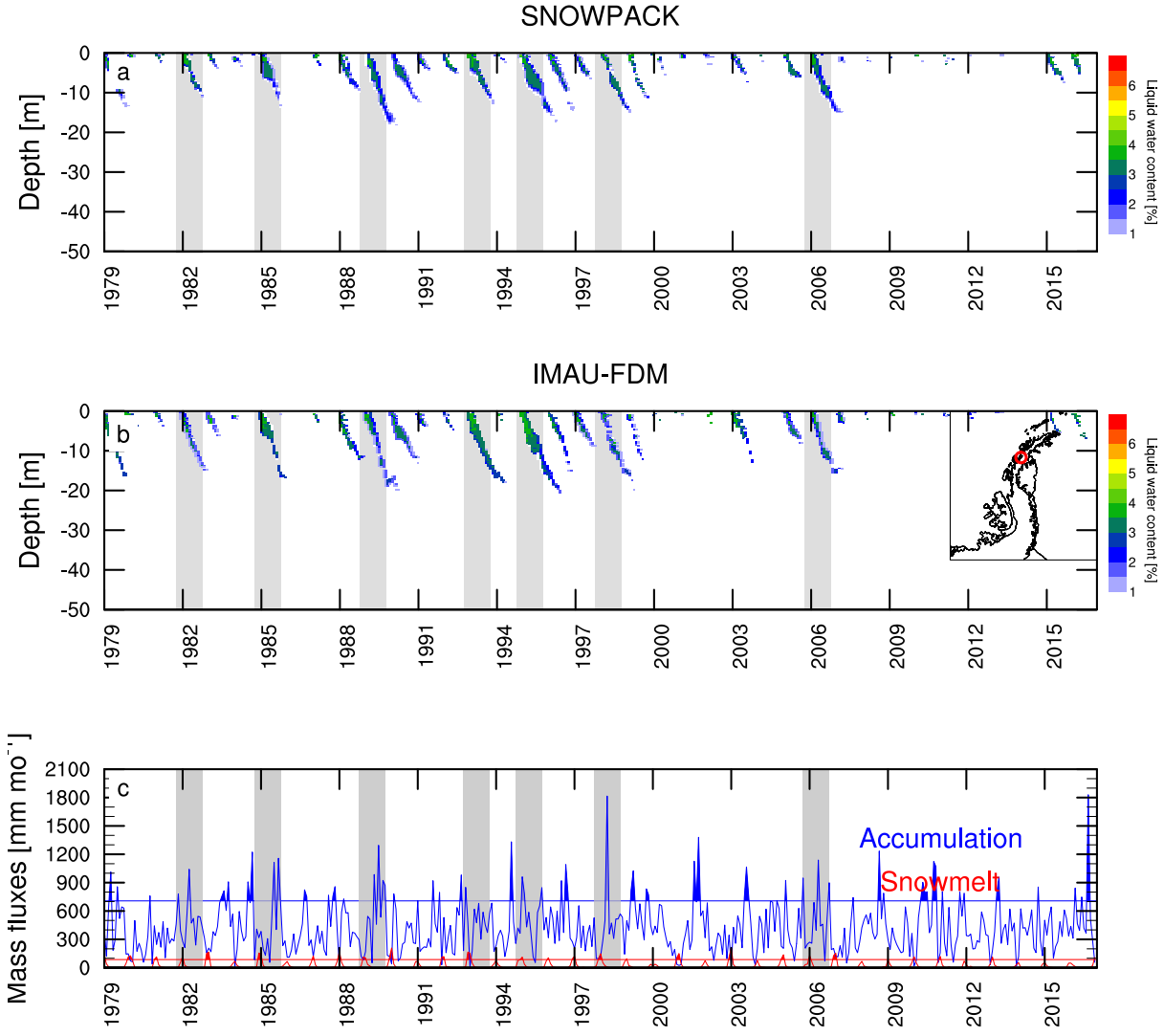


**Figure 12.** As for Fig. 9 but for a location in Palmer Land (see inset and Fig. 5).

https://doi.org/10.5194/tc-2020-148
Preprint. Discussion started: 14 July 2020


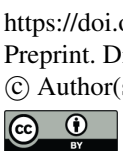

The Cryosphere
Discussions
Open Access
EGU

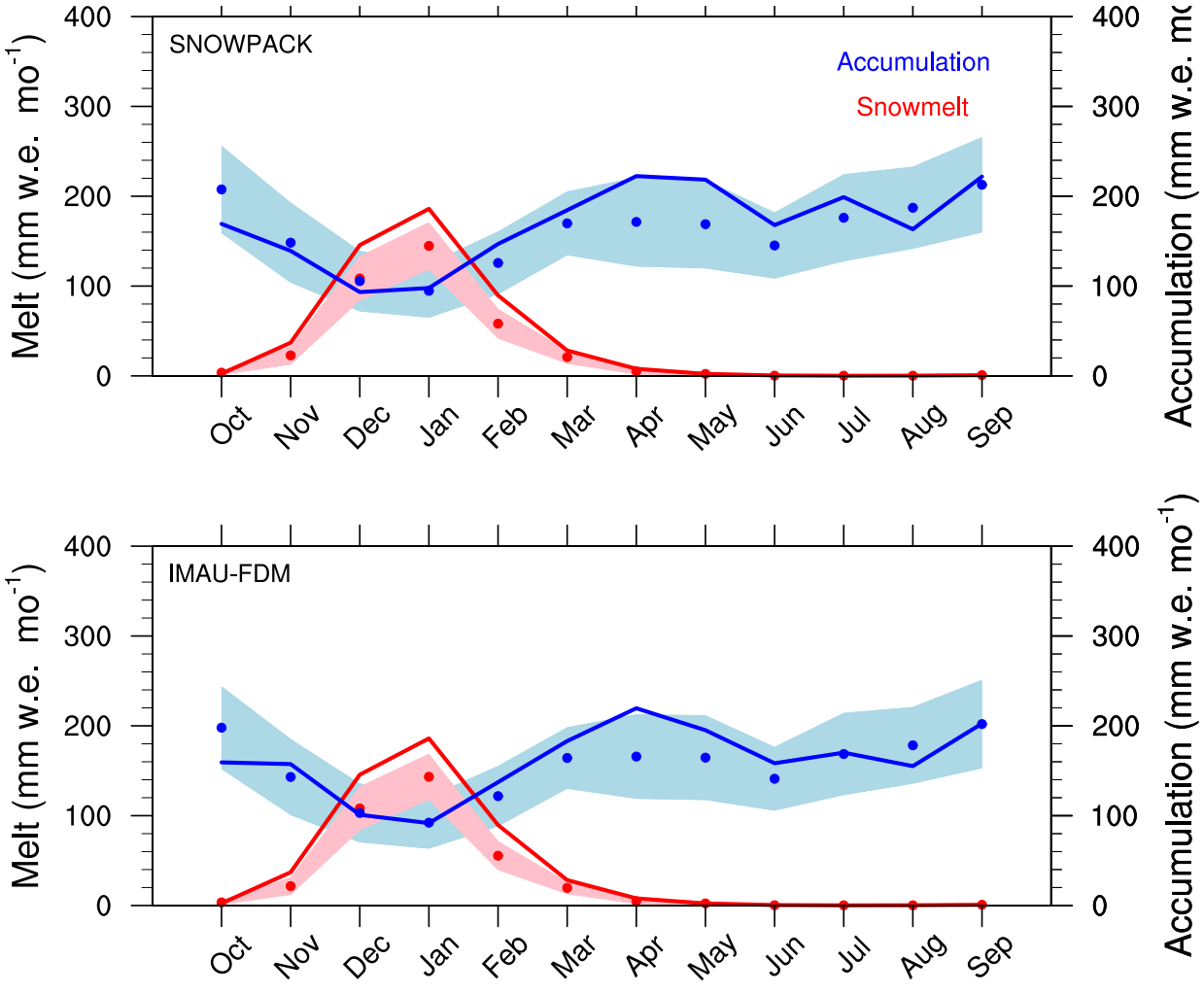


**Figure 13.** Monthly climatological (1979-2016) average surface melt production (left axis, red) and accumulation (right axis, blue) for years of >25% increases in perennial firn liquid water content. The solid lines show the monthly averages of formation years, while the dots show the monthly averages of all years in the 1979-2016 period.